JGR Earth Surface

RESEARCH ARTICLE
10.1029/2023JF007327

Stochastic in Space and Time: 2. Effects of Simulating Orographic Gradients in Daily Runoff Variability on Bedrock River Incision

A. M. Forte[1] and **M. W. Rossi**[2]

[1]Department of Geology and Geophysics, Louisiana State University, Baton Rouge, LA, USA, [2]Earth Lab, Cooperative Institute for Research in Environmental Sciences (CIRES), University of Colorado, Boulder, CO, USA

Key Points:

- Relationships among mean runoff and variability with topography in mountainous terrain can explain pseudo-thresholds in channel steepness
- Spatial asynchronicity of similar exceedance frequency runoff events is an unrecognized control on landscape evolution
- Orographic patterns in variability, snowmelt, and the characteristic size of runoff events alter predictions of climate-tectonic coupling

Supporting Information:

Supporting Information may be found in the online version of this article.

Correspondence to:

A. M. Forte,
aforte8@lsu.edu

Citation:

Forte, A. M., & Rossi, M. W. (2024). Stochastic in space and time: 2. Effects of simulating orographic gradients in daily runoff variability on bedrock river incision. *Journal of Geophysical Research: Earth Surface*, *129*, e2023JF007327. https://doi.org/10.1029/2023JF007327

Received 4 JULY 2023
Accepted 8 MAR 2024

Author Contributions:

Conceptualization: A. M. Forte, M. W. Rossi
Data curation: A. M. Forte
Formal analysis: A. M. Forte, M. W. Rossi
Investigation: A. M. Forte
Methodology: A. M. Forte, M. W. Rossi
Resources: M. W. Rossi
Software: A. M. Forte
Validation: A. M. Forte
Visualization: A. M. Forte
Writing – original draft: A. M. Forte
Writing – review & editing: M. W. Rossi

Abstract The extent to which climate and tectonics can be coupled rests on the degree to which topography and erosion rates scales linearly. The stream power incision model (SPIM) is commonly used to interpret such relationships, but is limited in probing mechanisms. A promising modification to stream power models are stochastic-threshold incision models (STIM) which incorporate both variability in discharge and a threshold to erosion. In this family of models, the form of the topography erosion rate relationship is largely controlled by runoff variability. Applications of STIM typically assume temporally variable, but spatially uniform and synchronous runoff generating events, an assumption that is likely broken in regions with complicated orography. To address this limitation, we develop a new 1D STIM model, which we refer to as spatial-STIM. This modified version of STIM allows for stochasticity in both time and space and is driven by empirical relationships between topography and runoff statistics. Coupling between mean runoff and runoff variability via topography in spatial-STIM generates highly nonlinear relationships between steady-state topography and erosion rates. We find that whether the daily statistics of runoff are spatially linked or unlinked, which sets whether there is spatial synchronicity in the recurrence interval of runoff generating events, is a fundamental control on landscape evolution. Many empirical topography—erosion rate data sets are based on data that span across the endmember scenarios of linked versus unlinked behavior. It is thus questionable whether singular SPIM relationships fit to those data can be meaningfully related to their associated hydroclimatic conditions.

Plain Language Summary Tectonic activity has long been known to modify climate by constructing mountain topography. Perhaps less obvious is the question of whether climatically driven erosion can also modify tectonic activity. This latter causal chain is premised on the notion that higher uplift rates can lead to steeper topography, higher precipitation rates, and thus more vigorous erosion. However, many erosion rate studies suggest that topography is only weakly sensitive to changes in rock uplift rates, thereby posing an important challenge to the climate-tectonic coupling hypothesis. Prior studies suggests that variability in daily runoff may be central to understanding this sensitivity, though historically have focused on how runoff is variable in time and not in space. As such, we developed a new numerical model of river erosion that simulates spatial patterns in runoff generation. We ran a suite of numerical experiments based on observed relationships among runoff, runoff variability, and topography to better understand how new model elements affect model sensitivity. We found that our crude representation of the size of runoff events is fundamental to model behavior. Given that event size is rarely considered in studies of climate-tectonic coupling, we argue that this property of runoff events requires more careful consideration.

1. Introduction

1.1. Motivation

The potential for two-way coupling between climate and tectonics is premised on how climate, erosion, and topography are related. Stream power provides an effective way to model the role of climate on erosion via a single parameter, the erodibility coefficient (Howard, 1994; Whipple & Tucker, 1999). When stream power is used as the principal erosion law, landscape evolution studies predict that climate should strongly influence the pattern and style of deformation in mountain belts (Beaumont et al., 1992; Whipple & Meade, 2006; Willett, 1999). These numerical models show how prevailing wind direction, along with an orographic enhancement of precipitation, leads to across-strike asymmetry in the efficiency of erosion of the landscape. However, field verification of such dynamics has been elusive, with ambiguous evidence both for and against coupling between

mean precipitation and tectonics (see discussion in Whipple, 2009). One barrier to field verification is uncertainty in how well suited stream power predictions are for isolating relationships among climate, erosion, and bedrock river morphology. Given the proliferation of carefully curated data sets attempting to constrain how climate is embedded in the erodibility coefficient (e.g., Adams et al., 2020; Ferrier et al., 2013; Forte et al., 2022; Leonard et al., 2023b), the time is ripe to re-visit assumptions implied by conventional applications of stream power to landscape evolution studies, especially in the context of the complexities that result from spatial gradients in orographic precipitation (e.g., Anders et al., 2006, 2007; Bookhagen & Burbank, 2006; Bookhagen & Strecker, 2008; Roe, 2005; Roe et al., 2003).

Since development of these early landscape evolution models, a large body of work has refined our understanding of the strengths and limitations of stream power (see summary in Lague, 2014). We highlight three sets of insights: (a) Probabilistic assessment of floods are needed when erosional thresholds matter (Lague et al., 2005; Snyder et al., 2003; Tucker, 2004); (b) Orographic gradients in mean precipitation lead to spatially non-uniform patterns in runoff generation (Bookhagen & Strecker, 2008; Roe et al., 2002, 2003); and (c) Precipitation phase (i.e., rain vs. snow) mediates spatio-temporal patterns in runoff generation (Anders et al., 2008; Bookhagen & Burbank, 2010; Rossi et al., 2020). While there are a number of important limitations to using stream power (e.g., channel width scaling, tools-cover effects), we focus here on those related to the characteristic discharge assumption typically used in stream power, specifically that the mean or bankfull discharge can be used to explain the long-term evolution or river morphology (e.g., see Wolman & Miller, 1960 for arguments based on alluvial rivers). Under this view, the characteristic discharge is generated from a characteristic runoff along hillslopes as it accumulates downstream. If runoff generation is uniform within a watershed, then the characteristic discharge is simply the product of the characteristic runoff and drainage area. In simple stream power, this set of assumptions entails that nonlinear relationships between channel steepness and long-term erosion rates will reflect differences in the incision process setting the slope exponent, n (Whipple & Tucker, 1999).

However, if erosional thresholds matter, nonlinearity is also linked to the temporal variability of streamflow (Lague, 2014; Lague et al., 2005; Tucker, 2004). As such, there has been increasing interest in examining how such stochastic-threshold models (stochastic-threshold incision models (STIM)) of river incision can be applied to empirical relationships between equilibrium channel steepness and long term erosion rates (Campforts et al., 2020; Desormeaux et al., 2022; DiBiase et al., 2010; Forte et al., 2022; Marder & Gallen, 2023; Scherler et al., 2017). Yet there has been less attention given to how orographic gradients in temporal dynamics may similarly alter predictions from simple stream power. Given the wide range of empirical estimates for n reported in the literature (Harel et al., 2016), we argue that river incision models likely require more hydrologic realism (e.g., Deal et al., 2018) to explain observed nonlinearities between channel steepness and erosion rate. In particular, we expand on STIM by: (a) allowing for orographic gradients in the magnitude-frequency relationships that describe runoff to evolve with growing topography, and (b) probing the influence of enforcing that magnitude-frequency relationships in runoff be spatially synchronous, thereby altering the resultant probability distributions of streamflow. We refer to this new 1D model of river profile evolution as spatial-STIM.

1.2. Approach and Scope

The basis for our work is the stochastic-threshold incision model (STIM) proposed by Lague et al. (2005), which itself drew heavily from prior modeling efforts (Tucker, 2004; Tucker & Bras, 2000). We consider a modified version of STIM whereby daily discharge distributions are treated as Weibull distributions instead of exponential or inverse gamma distributions (following Forte et al., 2022). As originally conceived, this river incision model uses the shear stress formulation of stream power as the instantaneous incision law. The equilibrium steepness of a longitudinal profile for a given rate of base level (BL) fall is then derived by integrating the product of the instantaneous incision law and the probability distribution of flows, with a lower bound of integration set by the erosion threshold. The original form of the Lague et al. (2005) model was zero-dimensional such that the scaling relationship between discharge and drainage area was fixed. When applied to a 1D river profile or a 2D drainage basin, this formulation applies (a) to bedrock rivers at equilibrium and (b) where STIM parameters are spatially invariant within the watershed. While there are many hard-to-constrain parameters in STIM, this model improves on the stream power incision model (SPIM) by explicitly showing how two hydroclimatic parameters, the mean runoff and a shape parameter describing the distribution of streamflow events, alter the form of the relationship between long-term denudation rates and channel steepness (DiBiase & Whipple, 2011; Lague et al., 2005). While interpreting mean runoff is intuitive, the shape parameter is less so. In short, the shape parameter describes the

variability of streamflow. While we describe this parameter more fully below, we highlight here that a key simplifying assumption in STIM is that runoff generating events are stochastic in time but not in space. For small catchments with relatively uniform surface properties, this is a reasonable assumption. As the size of watersheds increases and as surface properties become more heterogeneous, the potential importance of partial source areas for runoff generation during events are expected to become more important (Dunne & Black, 1970). This is likely exacerbated in high-relief landscapes where orographic effects lead to significant spatial and temporal variation in precipitation events (e.g., Anders et al., 2006, 2007; Barros et al., 2000; Campbell & Steenburgh, 2014; Frei & Schär, 1998; Minder et al., 2008). It is not our intention to embed a full hydrological model of event-scale runoff generation into a 1D profile model of river incision. Instead, we seek to add flexibility to STIM such that we can explore how runoff statistics that vary in *both* space and time alter model predictions.

There are four key novelties to our new 1D model of bedrock river incision, which we refer to as spatial-STIM. First, the simulated longitudinal profile is subdivided into uniform bins of stream distance that allow us to evolve orographic gradients in runoff statistics as the river profile changes. Second, both mean runoff and daily runoff variability are dictated by their relationship to topography, specifically in response to local relief and elevation. Third, these topography-hydrology relationships are based on relationships observed in modern mountain ranges, which are described in our companion manuscript to this one (Forte & Rossi, 2024b), thus explicitly considering the role of snowmelt in modulating runoff variability. Fourth, the temporal stochasticity of each bin can either be linked or unlinked spatially. In other words, the recurrence probabilities of daily events within bins are either synchronous (linked) or asynchronous (unlinked) along the river profile. Asynchronous runoff generation will lead to much different streamflow distributions as upstream stochasticity modifies the downstream accumulation of daily runoff. This last modification allows for examination into how the characteristic spatial scale of runoff events impacts model predictions.

We focus our analysis of model sensitivity to the new model elements introduced in spatial-STIM, the orographic rules used to set streamflow parameters, and changes in rock uplift rates. Our results are not intended to provide formal model calibration and validation using erosion rate data. Instead, our goal is to show how spatial-STIM might alter interpretations of the numerous channel steepness-erosion rate relationships reported in the literature and to develop heuristics for how such relationships might evolve as a mountain range grows (Figure 1). The conceptual framework builds on the findings from the companion manuscript to this one (Forte & Rossi, 2024b). That analysis revealed that both mean runoff and snowmelt fraction (SF) are functionally related to topography at the mountain range scale (Figure 1a). Increases in both are tied to a decreasing variability in daily runoff (Figure 1b), which itself is expected to cause increasingly nonlinear relationships between channel steepness and erosion rates (Figure 1c). As suggested by Forte et al. (2022), this set of expected relationships predicts an orographic feedback in which the continued topographic growth of a mountain range may be limited by the decreasing variability of streamflow and increasing nonlinearity in topography and channel steepness relationships (Figure 1). Consequently, we first ask what these dynamics entail for realistic gradients in mean runoff, runoff variability, and snowmelt. We then ask how the assumption of spatially synchronous runoff events (i.e., linked or unlinked per our definition above) may alter interpretations of river profile morphology. Questions are addressed by conducting a suite of numerical experiments using spatial-STIM.

2. Background

2.1. Channel Steepness and Erosion Rate Relationships

For river analysis, it is useful to define a channel steepness index (k_s) that accounts for the expected covariation of slope and drainage area within river systems (Flint, 1974):

$$k_s = A^{\theta} S \tag{1}$$

where A is drainage area [L^2], S is local river slope [L/L], and θ is a dimensionless constant that describes the concavity of the river profile. In order to compare channel steepnesses for rivers with different concavities, the steepness index k_s can be normalized by setting θ to a reference value, θ_{ref}, thereby defining a normalized channel steepness index, k_{sn} (Wobus et al., 2006). Normalized channel steepness can be determined via regression of the

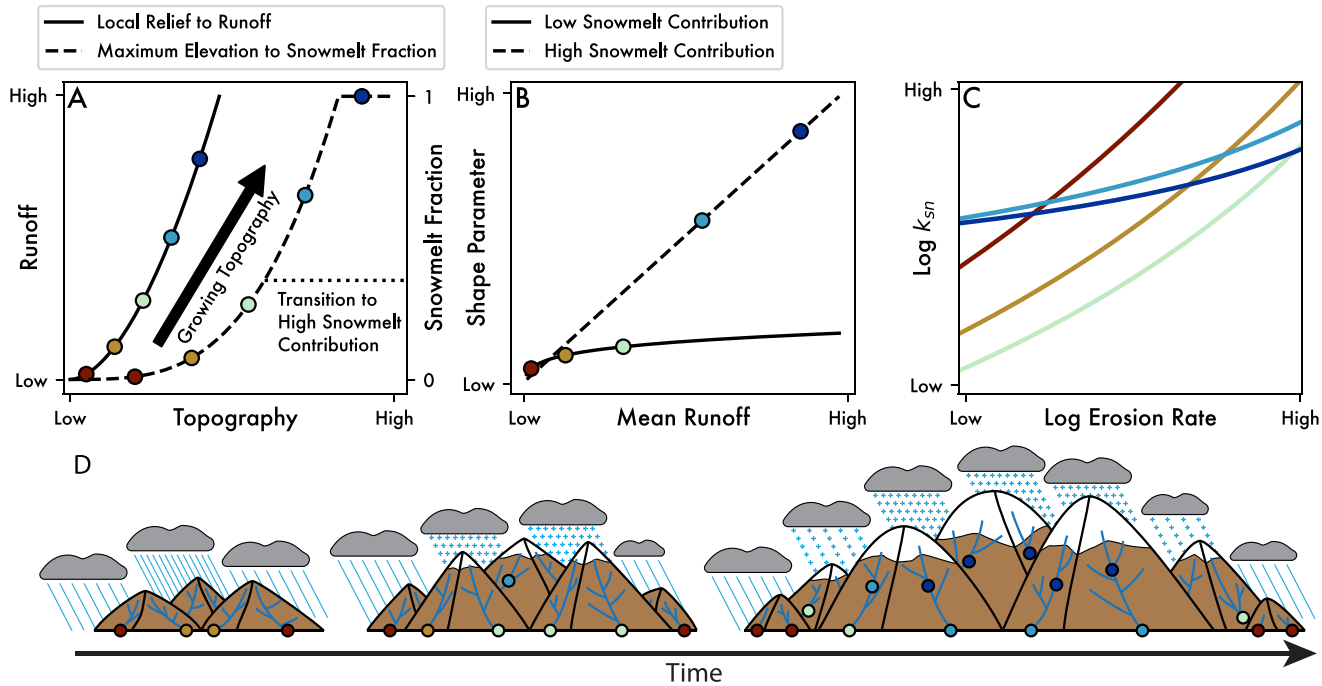

Figure 1. Conceptual model of how the covariation of topography, mean runoff, snowmelt fraction (SF) of runoff, and runoff variability might influence the k_{sn}-E relationship as topography grows, based on expectations from empirical relationships developed in Forte and Rossi (2024b). (a) Relationships between local relief and mean runoff (solid line) and maximum elevation and the fraction of runoff derived from snowmelt (dashed line). Horizontal dotted line indicates SF where runoff-variability relationships transition from a power law to a linear form. Colored dots represent hypothetical states as topography grows. (b) Relationship between mean runoff and variability. Solid line is a power law relationship that characterizes conditions when snowmelt contribution is low. Dashed line is a linear relationship that characterizes conditions when the snowmelt contribution is significant. (c) Implied k_{sn}-E relationships for the different mean runoff—variability relationships from (b). (d) Schematic envisioning how the relationships in panels (a–c) might evolve through time and space as a mountain range grows. The color of dots corresponds to colors shown in panels (a–c).

log-transformed, slope-area data along river profiles (Kirby & Whipple, 2012). However, it is now more common to use the so-called χ-transform to calculate k_{sn} because of the noise inherent in slope-area data (Whipple et al., 2022). As defined by Perron and Royden (2013), χ is an integral transform of distance such that:

$$\chi = \int_{x_b}^{x} (A_0/A(x))^{\theta_{\text{ref}}} dx \tag{2}$$

where A_0 is a reference drainage area, x is distance from the catchment outlet, and x_b is the position of the outlet. On a plot of χ and elevation, an equilibrium channel with a uniform k_{sn} appears as a straight line, assuming an appropriate θ_{ref} is used in the calculation of χ. When A_0 is set to one, the slope of the χ-elevation line equals k_{sn}.

Relationships between catchment-averaged normalized channel steepness and long-term erosion rates, E, show that: (a) k_{sn} tends to be positively correlated with average erosion rate, but that (b) the exact form of k_{sn}-E relationships varies substantially among landscapes (see compilations in Harel et al., 2016; Kirby & Whipple, 2012; Lague, 2014; Marder & Gallen, 2023). The general form of these relationships follow:

$$k_{sn} = CE^{\Phi} \tag{3}$$

where C and Φ are constants that vary between locations. To interpret these empirical relationships, it is common to recast Equation 3 in terms of the parameters used in the SPIM (Howard, 1994; Whipple & Tucker, 1999). SPIM considers erosion in terms of an erosional efficiency parameter (K) that encapsulates aspects of both climate and lithology, along with A and S:

$$E = KA^m S^n \tag{4}$$

where m and n are constants thought to represent details of the hydrological and erosional processes, respectively. In Equation 4, drainage area is a proxy for mean discharge $\bar{Q}$ [L^3/t] and implicitly assumes a simple relationship between mean discharge, mean runoff $\bar{R}$ [L/t], and drainage area such that $\bar{Q} = \bar{R}A$ and where $\bar{Q}$ and $\bar{R}$ are the characteristic discharge and characteristic runoff, respectively. The erosional efficiency parameter, K, embeds $\bar{R}^m$ thereby directly relating K to the hydroclimatology. By combining Equations 1, 3, and 4 in SPIM, it can be readily shown that:

$$\theta_{\text{ref}} = \frac{m}{n}, \tag{5}$$

$$C = K^{-1/n}, \tag{6}$$

$$\Phi = \frac{1}{n}, \tag{7}$$

and thus,

$$k_{sn} = K^{-1/n}E^{1/n} \text{ or } E = Kk_{sn}^{n} \tag{8}$$

Equation 8 predicts that the form of the k_{sn}-E relationship can be cast in terms of variations in climate and lithology (represented by K) and erosional process (represented by n). Implicit in this relationship are the assumptions that the basin-averaged value of k_{sn} and E are steady state values where the erosion rate approximately equals the long-term rock uplift rate and that the k_{sn} within the watershed in question is spatially uniform and free of transients (i.e., no prominent knickpoints).

Recently, it has been shown that relationships between channel steepness and erosion rates can be further interrogated by disentangling the climatic and lithologic components of the erosional efficiency parameter, K, by defining an alternate form of k_{sn} that includes a proxy for discharge. This new index, k_{snQ}, was defined by Adams et al. (2020):

$$k_{snQ} = \bar{Q}^{\theta_{\text{ref}}}S. \tag{9}$$

Calculations of k_{snQ} typically use mean precipitation as a proxy for mean runoff to calculate discharge, embedding the notion that mean runoff linearly scales with mean precipitation. Using the same assumption in Equation 3 that $\bar{Q} = \bar{R}A$, it is then possible to recast K as:

$$K = K_{lp}\bar{R}^m \tag{10}$$

where K_{lp} is the component of the erosional efficiency related to lithology and other factors such as sediment flux dynamics and erosion thresholds. The relationship between k_{sn}-E in Equation 8 can then be reformulated as:

$$k_{snQ} = K_{lp}^{-1/n}E^{1/n} \text{ or } E = K_{lp}k_{snQ}^{n} \tag{11}$$

This alternative formulation of channel steepness acknowledges spatially varying precipitation and runoff and thus should help reduce the role of climate in the steepness—erosion rate relationship, allowing both more accurate use of topography to estimate erosion rates (Adams et al., 2020) and isolation of lithologic controls on erosion rate (Leonard et al., 2023a, 2023b).

Interpretation of either k_{sn}-E and k_{snQ}-E relationships within a SPIM framework relies on a similar set of simplifying assumptions that have been articulated in more detail elsewhere (e.g., Harel et al., 2016; Kirby & Whipple, 2012; Lague, 2014). However, we highlight one important implication of SPIM to how the slope exponent in stream power, n, and the empirical exponent, Φ, are interpreted. Considering a steady state system where erosion rates balance uplift rates, the value of n controls the degree of nonlinearity, Φ (Equation 7). When $n \approx 1$, the linear relationship between topography and erosion rate implies that rivers maintain a uniform sensitivity to changes in rock uplift rate as they steepen. In contrast, when $n \gg 1$, and E is plotted on the abscissa,

the strongly sublinear relationship (i.e., very small values of Φ) between topography and erosion rate implies that channel steepness reaches a pseudo-threshold as uplift rates continue to increase. Consequently, higher values of n lead to a reduced potential for two-way coupling between climate and tectonics as topography is no longer able to adjust to increases in rock uplift rates (Whipple & Meade, 2004). Global compilations of k_{sn}-E suggest that $n \approx 2$ (e.g., Harel et al., 2016; Lague, 2014), implying a sublinear response, but not one where significant pseudo-thresholds in k_{sn} limits the relief of mountain landscapes (Hilley et al., 2019). However, at the individual landscape scale, substantial differences in the values of n are observed, with some locations suggesting more linear relationships (e.g., Ferrier et al., 2013; Safran et al., 2005; Wobus et al., 2006) while others exhibit strongly sublinear relationships (e.g., Cyr et al., 2010; Forte et al., 2022; Hilley et al., 2019). Diagnosing the underlying mechanisms for these large differences across landscapes is thus limited by relying on stream power alone.

2.2. Stochastic-Threshold Incision Model (STIM)

To probe controls on the nonlinear k_{sn}-E relationships described above, it is useful to consider an alternative fluvial incision model, specifically the stochastic-threshold incision model (STIM). STIM shares some similarities with SPIM, but adds two important modifications: (a) discharge magnitudes vary in time and (b) not all discharges are able to erode bedrock. While different variants of STIM have been presented (e.g., Snyder et al., 2003; Tucker, 2004), we focus on the version presented by Lague et al. (2005). The details of this model have been discussed in depth previously (e.g., Campforts et al., 2020; DiBiase & Whipple, 2011; Lague et al., 2005; Scherler et al., 2017), to which we refer interested readers. Nevertheless, we briefly present the governing equations here, focusing on differences from the original formulation of Lague et al. (2005).

STIM uses a stream power equation for instantaneous (e.g., daily) incision rates and then integrates the incision law over a probability distribution of daily discharges to calculate an average erosion rate. In the original formulation by Lague et al. (2005), both the instantaneous incision and average erosion rates were cast in terms of dimensionless discharge. For our application, it is more useful to define the instantaneous law in terms of a dimensional version of daily discharge (Q):

$$I = K k_{sn}^{n} \bar{Q}^{m-\gamma} Q^{\gamma} - \Psi_c \tag{12}$$

where γ is an exponent describing local discharge and Ψ_c is the threshold parameter. K, m, and n are similar to their counterparts in Equation 3, but have more formal definitions such that

$$K = k_e k_t^{a} k_w^{-a\alpha} \tag{13}$$

$$m = a\alpha(1 - \omega_a) \tag{14}$$

$$n = a\beta \tag{15}$$

$$\gamma = a\alpha(1 - \omega_s) \tag{16}$$

where k_e is a rock erodibility coefficient, k_t, α, and β are hydraulic and frictional constants, k_w, ω_a, and ω_s are constants related to channel width scaling with discharge, and a is an constant related to incisional process. The threshold parameter Ψ_c is related to both the rock erodibility and incisional process such that

$$\Psi_c = k_e \tau_c^{a} \tag{17}$$

where τ_c is the critical shear stress for initiating incision. To calculate an average, steady state erosion rate, E, Equation 12 must be integrated across a distribution of discharges

$$E = \int_{Q_c(k_{sn})}^{Q_m} I(Q, k_{sn}) \, \mathrm{pdf}(Q) \, dQ \tag{18}$$

where Q_c is the critical discharge above the incision threshold, Q_m is an arbitrarily high upper bound on discharge assuming that the integral is convergent, and the pdf(Q) is the probability distribution of daily discharge. In the original formulation of Lague et al. (2005), the inverse gamma distribution of normalized discharge was used, thus fixing the scale parameter to 1. Here, we follow recent work (Forte et al., 2022; Rossi et al., 2016) by using a two parameter Weibull distribution to describe daily statistics. Because we allow runoff to vary as a function of profile position which then accumulates downstream, our model simulates daily runoff distributions instead of streamflow ones:

$$\mathrm{pdf}(R;R_0,c_R)=\frac{c_R}{R_0}\left(\frac{R}{R_0}\right)^{c_R-1}\exp^{-1(R/R_0)^{c_R}} \tag{19}$$

where R_0 is a scale parameter, related to the mean of the distribution, and c_R is a shape parameter, describing the variability of daily runoff generation. Higher values of c_R imply lower variability. Because the original formulation was a zero-dimensional model, runoff variability and streamflow variability were equivalent, an important distinction that differs in our numerical model. The rationale for explicitly considering orographic gradients in runoff statistics is explained more fully in Section 4.

Prior studies using STIM highlight that the degree of linearity between channel steepness and erosion rate is strongly mediated by the discharge variability (DiBiase & Whipple, 2011; Lague et al., 2005; Tucker, 2004). Specifically, the value of Φ (Equation 7) is a function of the shape parameter of the daily discharge distribution when erosion thresholds are large with respect to erosion rates (Regime III in Lague et al., 2005). As such, one explanation of the wide range of empirical values for n and Φ might be due to regional differences in daily discharge variability (Marder & Gallen, 2023). Given that the shape parameters of inverse gamma and Weibull distributions are linearly related (Rossi et al., 2016), we are confident that the Weibull distribution can be reliably used in Equations 18 and 19. However, by using this alternative distribution, our modified version of STIM moderates the impact of heavy tailed distributions, allows discharge distributions to emerge from spatially variable runoff ones, and requires numerical simulation (i.e., there is no analytical solution).

3. Orographic Relationships Between Hydroclimatology and Topography

In our companion manuscript to this one (Forte & Rossi, 2024b), we used a 20-year global, daily time series of hydroclimate from the Water Global Assessment and Prognosis (WaterGAP3—Alcamo et al., 2003; Döll et al., 2003) along with the HydroSheds v1, 15 arcsecond digital elevation model (Lehner et al., 2008) and SRTM-90 data (Farr et al., 2007) to develop empirical relationships between hydroclimatological and topographic variables. We refer interested readers to Forte and Rossi (2024b) for more details, but summarize the primary results of that analysis here (Figure 2). Specifically, Forte and Rossi (2024b) found a similar inverse correlation between $\bar{R}$ and variability (Figure 2a) as identified in smaller data sets from gauged watersheds (e.g., Molnar et al., 2006; Rossi et al., 2016). The form of the relationship between $\bar{R}$ and variability is mediated by the relative contribution of snowmelt to total runoff (Rossi et al., 2016). The snowmelt fraction, SF, is the total amount of runoff from snowmelt divided by the total runoff. A distinct change in the functional form of this relationship occurs at a SF of ~0.35. When SF is relatively low, the relationship between $\bar{R}$ and c_R is more nonlinear than when SF is high (Figure 2a).

Because the shape (c_R) and scale (R_0) parameters shown in Figure 2 were determined by fitting the right tail of runoff distributions above a 1% threshold, these fit parameters are no longer related to the mean of the distribution in a simple way (Forte & Rossi, 2024b). The scale parameter from the fits of daily data (R_0) is linearly related to the scale estimated from the mean runoff ($R_0{}^*$) using the general equation for a Weibull distribution:

$$R_0{}^*=\frac{\bar{R}}{\Gamma(1+1/c_R)} \tag{20}$$

But deviates substantially from the 1:1 line, especially in snowmelt influenced settings (Figure 2b). To account for this in our numerical model, we use the relationship between R_0 and $R_0{}^*$ (Figure 2b) to estimate the appropriate R_0 from the calculated $R_0{}^*$ based on the appropriate mean runoff and c_R for a given bin.

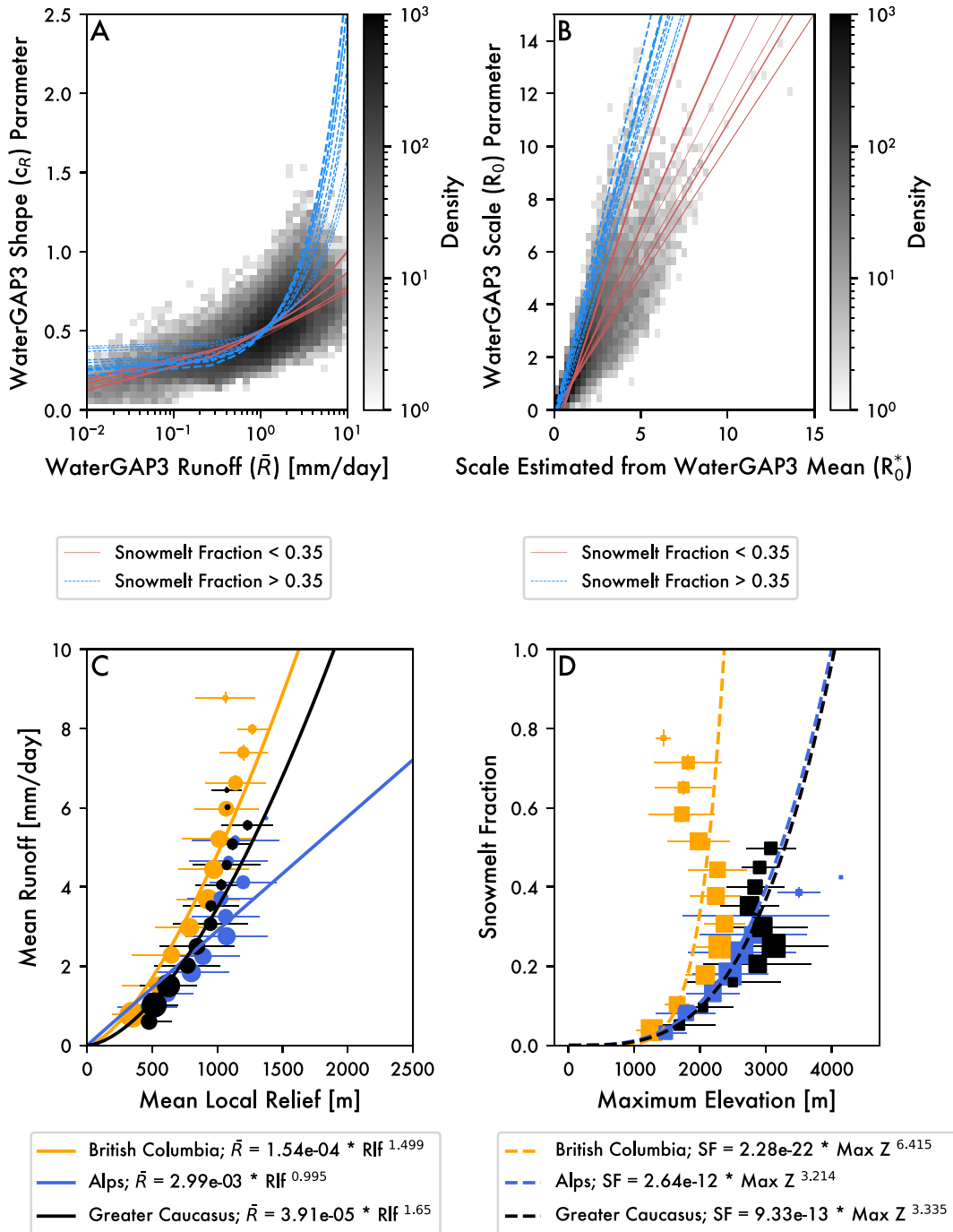

Figure 2. Summary of empirical results from Forte and Rossi (2024b) relate topography and hydroclimatological variables of interest. (a) Relationship between mean daily runoff ($\overline{R}$) and daily runoff variability as parameterized by the Weibull shape parameter (c_R). Colored lines indicate individual fits to $\overline{R}$ and c_R within bins of snowmelt fraction (SF). Red solid lines are power law fit for bins with SF < 0.35 and blue dashed lines are linear fits for bins with SF > 0.35. (b) Relationship between the scale parameter implied by the mean runoff and that fit to the runoff distributions above an exceedance threshold. Symbology is similar to A but lines show linear regressions. (c) Power law fits between mean local relief and $\overline{R}$ for three regional examples using WaterGAP3 data. (d) Power law fits between maximum elevation and SF for three regional examples using WaterGAP3 data. In both C and D, the symbols are scaled to the number of observations and whiskers show one standard deviation. More details on regressions for each panel can be found in Forte and Rossi (2024a, 2024b).

Our main aim in the numerical modeling is to evolve stochastic runoff parameters as mountain topography grows. In order to uniquely prescribe the distribution of flows (e.g., Equation 19) within a part of a river profile, we need to know both $\bar{R}$ and SF so that we can modify $R_0{}^*$ and c_R. As described in Forte and Rossi (2024b), identifying singular, global relationships between either $\bar{R}$ or SF and topographic metrics is challenging. As such, we use the three regional relationships between mean local relief and $\bar{R}$ and maximum elevation and SF in the Greater Caucasus, European Alps, and northern British Columbia (Figures 2c and 2d). It is worth emphasizing that the lack of global relationships between either $\bar{R}$ or SF and topography implies that rules for how runoff statistics coevolve with mountain growth needs regional constraints. However, the similar forms of these relationships is not surprising given prior work showing how local relief sets orographic precipitation (e.g., Bookhagen & Burbank, 2006; Bookhagen & Strecker, 2008). Furthermore, the increasing importance of snowmelt as mountain ranges grow is grounded in physical theory (i.e., typical temperature lapse rates imply decreasing temperatures with elevation and thus a potential for increasing snow fraction with elevation).

The two topographic metrics we focus on are local relief and local maximum elevation (e.g., within a WaterGAP3 pixel). While these topographic metrics are thought to be linked to river morphology at certain spatial scales (e.g., Ahnert, 1970), how to best use them to drive rules in a 1D river incision model is not obvious. Given our discretization of river profiles into bins, we argue there is a sensible way to honor the empirical relationships we show in Figure 2 into a 1D river incision model. For example, it has been shown that local relief at the 2–2.5 km radius scale is linearly correlated with channel steepness (e.g., DiBiase et al., 2010). Channel steepness is a property of the river profile that can be readily calculated (Equation 1) and updated as the river profile evolves through time. How local relief is related to channel steepness for our three selected regions is developed using the methods described in Forte et al. (2016), which itself uses a combination of TopoToolbox (Schwanghart & Scherler, 2014) and the Topographic Analysis Kit (Forte & Whipple, 2019). First, we extract all watersheds with a drainage area >50 km^2 and an outlet elevation above 300 m. Any watershed from this initial extraction with a drainage area >250 km^2 was then subdivided into tributary watersheds that connect to the trunk channel using drainage areas >50 km^2 as a threshold. For each catchment, mean channel steepness and local relief (2,500 m radius) was calculated along with the R^2 value for a linear fit between χ (Equation 2) and elevation. Values of R^2 close to 1 imply that a river profile is largely free of major knickpoints. The R^2 values were thus used to screen for reaches in quasi-equilibrium such that only reaches above a high threshold (>0.90; Figure S1 in Supporting Information S1) were used to develop regionally based relationships between channel steepness and local relief. By establishing the channel steepness to local relief relationship for each site, we can then apply these rulesets based on local relief into our river incision model. It is worth noting that, in this transformation, we used a relationship between k_{sn} and 2.5 km relief (as described above) using SRTM-90 data. In contrast, the relationship between mean runoff and 2.5 km relief used the HydroSheds 15-s data (Figure 2c). For our regions of interest, the distributions of these two local relief data sets do not suggest meaningful differences (Figure S1 in Supporting Information S1). As channel steepness evolves in the numerical model, it is directly tied to local relief and indirectly tied to maximum elevation, the latter of which is calculated by adding the local relief to the minimum elevation of the profile for a given bin. The choice of using the lowest maximum elevation is a conservative one because it produces the smallest possible SF for a given value of local relief.

4. River Incision Model

There are now many studies testing the utility of the STIM (e.g., Campforts et al., 2020; Desormeaux et al., 2022; DiBiase & Whipple, 2011; Forte et al., 2022; Marder & Gallen, 2023; Scherler et al., 2017). However, we believe this paper is the first attempt to modify a longitudinal profile version of STIM to allow for stochastic events in space as well as time, which we refer to as spatial-STIM. Our modeling strategy shares some similarity with recent 2D efforts that consider the role of spatial variability in precipitation events (e.g., Coulthard & Skinner, 2016; Peleg et al., 2021), but these efforts considered landscape evolution at timescales orders of magnitude shorter than we do here. By subdividing the long profile into bins we coevolve the hydrology with the local channel morphology. Using a binned approach requires a decision for whether spatial bins should depend on each other (i.e., the recurrence interval of runoff events on a given day are synchronous across the profile) or whether they should be treated independently (e.g., bins experience storm or snowmelt events of different recurrence intervals at a given time). We refer to the former as linked cases and the latter as unlinked ones, referring to whether the recurrence intervals between bins are linked to each other or unlinked. In both linked and

unlinked cases, the profiles experience orographic gradients in mean daily runoff and daily runoff variability. We further describe the nuances of linked versus unlinked cases in Section 4.2.

4.1. Spatial-STIM

Our new 1D river profile bedrock incision model was developed in Python 3.10 by implementing an explicit upwind finite difference solution of Equation 12 for daily incision along the profile. The model itself is available from Forte (2024). The starting condition for each model run uses a drainage area distribution based on the relationship between profile length (L) [L] and drainage area (A) [L^2] from Sassolas-Serrayet et al. (2018):

$$L = cG_cA^{n_A} \tag{21}$$

$$c = 0.5G_c\sqrt{\pi} + 0.25\sqrt{G_c^2\pi - 4} \tag{22}$$

where G_c, or the Gravelius coefficient, is set to 1.5 and the exponent n_A is set to 0.54. This form of the relationship between drainage area and stream distance is useful because it allows for direct consideration of the shape of the drainage basin using a single parameter. A watershed with a G_c of 1 has a perfectly circular boundary and a watershed with a G_c of 2 is a narrow, elongated watershed. Because we are only simulating the river profile, we use a threshold drainage area, A_c, of 1 km^2. Using the specified G_c and n_A from above, this is equivalent to the Hack (1957) relationship

$$A = k_aL^h + A_c \tag{23}$$

where $k_a = 0.969$ and $h = 1.851$. For all runs, we set the spacing between nodes at 100 m and the time step to one day, with saved outputs every 5,000 years. All runs are initialized using a profile with a low and constant k_{sn} of 25 m.

Spatial variations in both mean runoff and runoff variability are handled by adopting uniform river length bins along the longitudinal profile. This implies that the proportion of total drainage area represented by each bin varies along the profile. We test the sensitivity of the model to this style of discretization in Section 5.3. Each bin has a single scale and shape parameter describing the runoff distribution that is used for all the nodes within the bin. At each time step, these parameters are recalculated based on the current topography. Figure 3 shows an example of how the mean runoff and shape parameter vary as a function of bin location at one time step during a transient. The location and dimensions of bins are fixed for each model run to maintain computational efficiency. However, our analysis of model sensitivity includes varying the bin size and number of bins within a profile to test the sensitivity of results to these choices (see Section 5.3). The key property of our model that allows hydroclimatology to coevolve with the topography occurs in the method we use to the recalculate the shape and scale parameters at every time step.

As described in Section 3, we used both global (Figures 2a and 2b) and regional relationships (Figures 2c and 2d) to define the mean runoff, scale parameter, and shape parameter within each bin. For a given time step and bin, the chain of action is: (a) Use the channel steepness from the previous step to calculate local relief using the linear relationships developed from the SRTM-90 elevation data (e.g., Figure S1 in Supporting Information S1); (b) Use the local relief to calculate mean runoff using the power law relationships developed from the regional WaterGAP3 analysis (Figure 2c); (c) Also use the local relief to determine the maximum elevation by adding it to the minimum elevation within the bin; (d) Use the maximum elevation to calculate the SF using the power law relationships developed from the regional WaterGAP3 analysis (Figure 2d); and finally (5) Use the SF to choose an appropriate mean runoff and shape parameter (Figure 2a) and do the scale parameter adjustment (Figure 2b) based on the global WaterGAP3 analysis. In this way, the mean runoff, scale, and shape parameters are updated from channel topography alone and follow data driven rules.

To ensure that the model does not extrapolate into an unreasonable part of parameter space, we impose a maximum relief that any bin can achieve. We set this to 2,500 m for most runs based on a conservative estimate of what is observed in modern landscapes (e.g., Figure S1 in Supporting Information S1), though we also test the sensitivity of model results to this choice in Section 5.3. The imposition of a maximum relief is

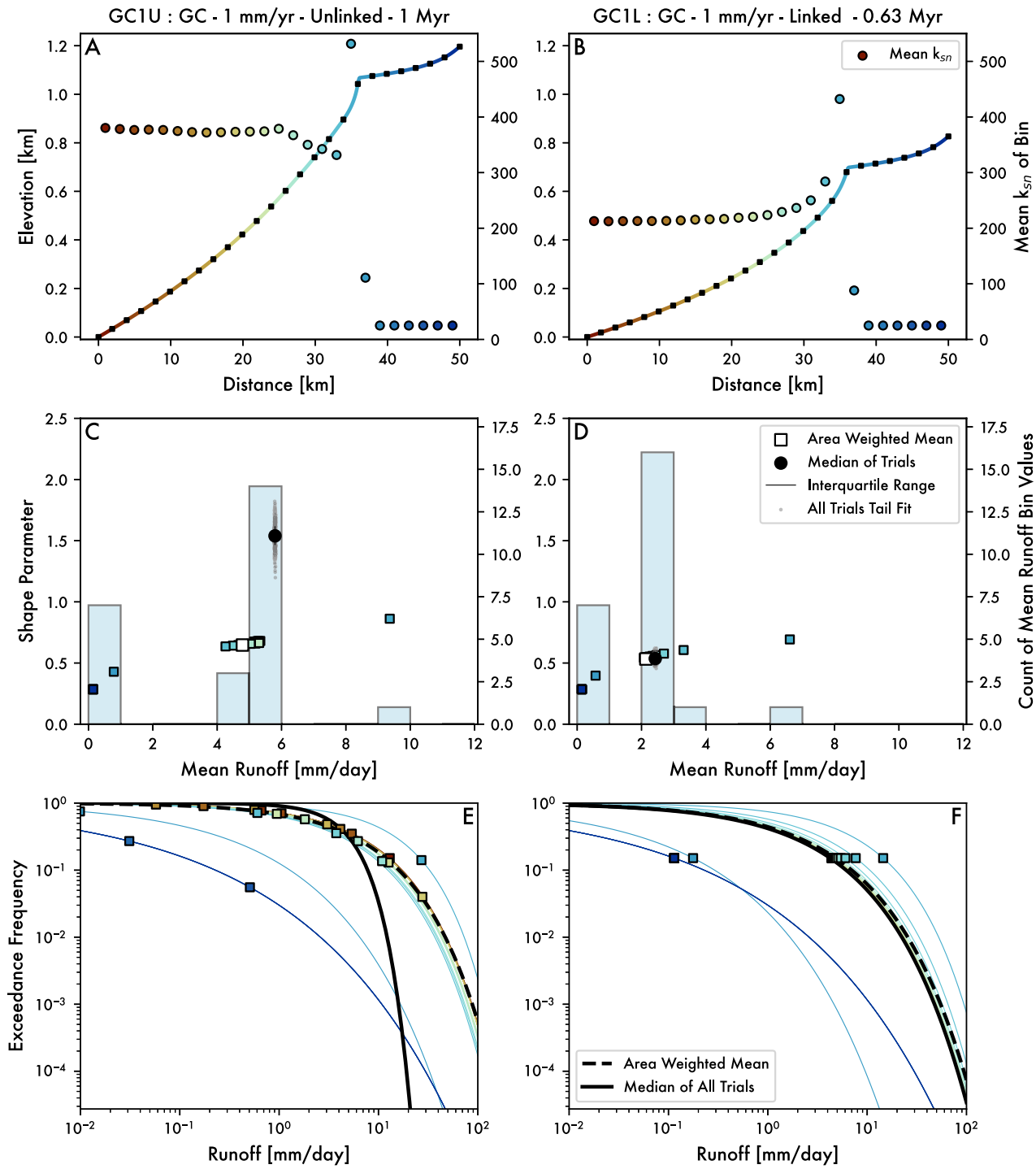

Figure 3. (a) Longitudinal profile of unlinked model GC1U at 1 Myr into the model run (colored line with black squares), where colors indicate individual bins and black squares mark bin boundaries. Also shown is the mean k_{sn} for each bin (colored circles) (b) Same as in A but for linked model GC1L at 0.63 Myr into the model run, which represents a comparable point in the transient response. (c) Mean runoff and variability for GC1U at 1 Myr. Colored squares are mean runoff and variability for the individual bins. White square is runoff and variability from a drainage area weighted mean of the bins. The black circle is the median of 500 trials of mean runoff and variability from routing 100 years of discharge for each trial, where small gray dots are mean runoff and variability for individual trials. This is overlain on a histogram of the runoff within bins to emphasize that many of the bins have runoffs clustered around the mean. (d) Same as in C but for model GC1L at 0.63 Myr. (e) Exceedance frequency plot for GC1U at 1 Myr, showing the probability distributions for individual bins as thin colored lines, the area-weighted mean runoff and variability as the black dashed line, and the mean runoff and variability from the median of the 500 trials as the black solid line. The colored squares represent runoff for each individual bin on a random day. (f) Same as E but for model GC1L at 0.63 Myr. Note that the difference between the assortment of frequencies and runoffs on the random days (small squares) between (e) and (f) result from (e) being an unlinked model and (f) being a linked model. Because (f) is linked, the runoff magnitude for the random day shown all plot at a single recurrence interval.

broadly motivated by limits to local relief set by hillslope strength (e.g., Montgomery & Brandon, 2002; Schmidt & Montgomery, 1995). Embedded in the assumption of a maximum local relief is the expectation that this should be controlled by processes not considered in our model (e.g., hillslope creep or mass wasting). While we do not impose a limit on maximum elevation, it has an implicit limit set by the local relief maximum. We also make sure that the SF cannot exceed 1. After meeting all these constraints, each bin has a scale and shape parameter describing the probability distribution of runoffs expected for each bin at a given time step (e.g., Figure 3). To simulate the stochasticity implied by these derived parameters, we use the *SciPy weibull_min* and appropriate sub-functions to randomly extract a runoff magnitude from the relevant probability distribution for that bin. In detail, for every 100 years of model run time, the model generates a 100 years daily time series (i.e., 36,500 days) of runoffs within each bin. This is done for efficiency because the random selection of numbers from a distribution is one of the more computationally time intensive steps. The compute time required to generate one random number is comparable to generating a large quantity of random numbers from a given distribution. The impact of this decision means that mean runoff and variability are only updated every 100 years. However, even for the maximum 8 mm/yr rock uplift rate we impose, the amount of profile change - and thus change in either relief or maximum elevation - in 100 years is sufficiently small as to not significantly influence results. At each 100-year increment where the runoff time series is generated, the current iteration number is used as the starting seed for the generation of subsequent random numbers. This ensures that the random numbers (i.e., runoff magnitudes) change through the model run.

For each day, runoff within each bin is first routed along the profile before calculating fluvial incision. Specifically, on a given day and within each bin along the stream profile, a random magnitude of runoff is drawn from the runoff distribution for that bin. Any stream nodes within that bin are assigned that runoff magnitude. This is done for all bins. Then, at each node, the daily runoff [L/T] is converted into a volume by multiplying by the drainage area (A) contributed by that node (i.e., dA/dx). The volumes within each node are cumulatively summed downstream to convert to daily discharge (Q) for use in the finite difference solution of Equation 12. An identical procedure is performed using the mean runoff in each bin (base on the relevant regional relationship between mean runoff and mean local relief) to generate a mean discharge ($\bar{Q}$) for use within Equation 12.

4.2. Linked Versus Unlinked Cases

Whether neighboring bins are correlated or independent in time depends on how runoff events are generated in the landscape. The spatially correlated case mimics scenarios where storm or snowmelt runoff events vary in magnitude along the profile but represent the same recurrence interval (linked). The spatially independent case mimics scenarios where storm or snowmelt runoff events also vary in magnitude along the profile but where the runoff magnitudes are randomly drawn from the probability distributions for each bin independent of each other (unlinked). It is critical to clarify that both the linked and unlinked cases produce along-profile gradients in runoff magnitudes that coevolve with growing topography (e.g., see example probability distributions in Figure 3f). Linking the probability of events within bins along the profile enforces that runoff is spatially autocorrelated and is analogous to asserting a nonlinear scaling between streamflow and drainage area in prior treatments of STIM. In contrast, the unlinked case allows for crude assessment of the relative scales between runoff source areas and the size of basin. By specifically considering the two endmember scenarios where exceedance probabilities are either uniform (linked) or independent (unlinked) across the basin, we are able to evaluate the potential importance of spatial autocorrelation in daily runoff on the efficiency of erosion. We consider how to physically interpret linked and unlinked cases in Section 6.2.2, but it is important to emphasize that with respect to the model setup, we are largely agnostic as to possible physical or hydroclimatological processes these two endmembers represent. This agnosticism includes the somewhat generic terminology we adopt for these two scenarios, that is, linked versus unlinked, to avoid association of them with any specific process as we expect that there are non-unique sets of process interactions that can lead to these behaviors. Finally, we emphasize that these two behaviors are extreme endmembers, and we would fully expect most real landscapes to behave as a mixture of these two endmembers.

Implementation of the unlinked versus linked scenarios is set by changing the pseudorandom seed number. For a given seed number, the pseudorandom number generator will produce a reproducible sequence of numbers. In the linked scenarios, the seed for the 100-year time series is set by the iteration number for all bins. In the unlinked

case, the seed number for bins are incremented by 1, such that for bin 1, the seed is i, for bin 2, the seed is $i + 1$, and so on. For the linked cases, this forces the exceedance frequency of events in all bins to be identical at a given timestep (e.g., Figure 3f). For the unlinked cases, this allows the exceedance frequency of events in bins to vary at a given timestep (e.g., Figure 3e). In the unlinked case, the size of the bins crudely represents an assumed characteristic size of runoff events. Real landscapes likely experience a mixture of small footprint, convective rain events, large footprint, synoptic-scale rain events, temperature-induced snowmelt events, and rain-on-snow events. For example, in our companion manuscript (Forte & Rossi, 2024b), we showed how the largest area runoff events above a given magnitude tend to be increasingly produced by snowmelt. We anticipate that mixtures of event sizes, like those suggested by the WaterGAP3 data, will produce intermediate behaviors and response times, which is why we consider both the linked and unlinked endmember scenarios for all parameter sets. The question of whether landscapes are better represented by unlinked versus linked scenarios is revisited in the discussion.

4.3. Model Parameterization

Our main objectives in this study are to extend the zero-dimensional stochastic-threshold incision model (STIM) of Lague et al. (2005) to a 1D profile model that includes spatially varying daily runoff variability (spatial-STIM). The purpose of this new model is to see how coupling orographic patterns in runoff variability can alter predictions in the steady state and transient evolution of river longitudinal profiles using stream power. It is beyond the scope of this effort to do a full sensitivity analysis on all the STIM parameters, which have already been explored in great depth (DiBiase & Whipple, 2011; Lague, 2014; Lague et al., 2005). Instead, we focus on driving our new model using empirical relationships for how mean runoff and daily runoff variability vary as a function of local relief and testing the sensitivity of our results to the differences in model structure we have added to spatial-STIM. As such, most STIM parameters (like thresholds, rock erodibilities, width scaling) are fixed in all model runs, typically to values that were used in our prior work in the Greater Caucasus (Forte et al., 2022). The values of fixed parameters are reported in Table S1 in Supporting Information S1. Table S2 summarizes the parameters we vary in our numerical experiments and contains a complete list of model runs. The suite of numerical experiments we conduct address two central questions: (a) What do orographic relationships between mean runoff and daily runoff variability entail for STIM-based predictions of the relationship between channel steepness and rock uplift rates, and (b) How sensitive are spatial-STIM results to the new elements of model structure (i.e., by varying stochastic parameters along bins in the longitudinal profile)?

5. Results

We report results in three parts. The first part provides results for a series of baseline cases that use a similar model structure (50 km long rivers, 2 km wide bins), albeit for both the linked and unlinked scenarios. These baseline cases represent how a ~488 km^2 area watershed responds to range of uplift rates (0.25–8 mm/yr) under modern hydroclimatic conditions of the mountainous regions of the Greater Caucasus, European Alps, and British Columbia. The second part uses the results from the Greater Caucasus runs to interrogate the large differences in transient and steady state behavior that are observed between linked and unlinked cases. Specifically, we examine when and where erosional thresholds are exceeded. The third part tests the sensitivity of our findings to other differences in model structure, specifically to profile length, bin size, bin number, maximum local relief, and binning criteria. To do this, we use the linked Greater Caucasus baseline case at rock uplift rates of 1 mm/yr as the starting point for the majority of sensitivity analyses. Sensitivity experiments vary: (a) stream length and number of bins using model setups of 10, 20, 30, 40, 50, and 100 km width bins fixed at 2 km wide, (b) maximum relief within a bin using model setups of 1,500, 2,000, and 2,500 m, and (c) bin size using model setups of 2, 5, and 10 km wide bins. Because profile length and bin size together define the number of bins, we also run a sensitivity experiment designed to: (d) test the notion that number of bins, and thereby the granularity of how we represent the hydroclimate, is controlling the steady state channel steepness. This latter test compares two profile lengths of 10 and 50 km long using both 5 and 10 bins. Finally, we test the sensitivity of the model results to the binning scheme by: (e) running a full suite of models where we divide the profile into bins of equal drainage area as opposed to equal stream distance.

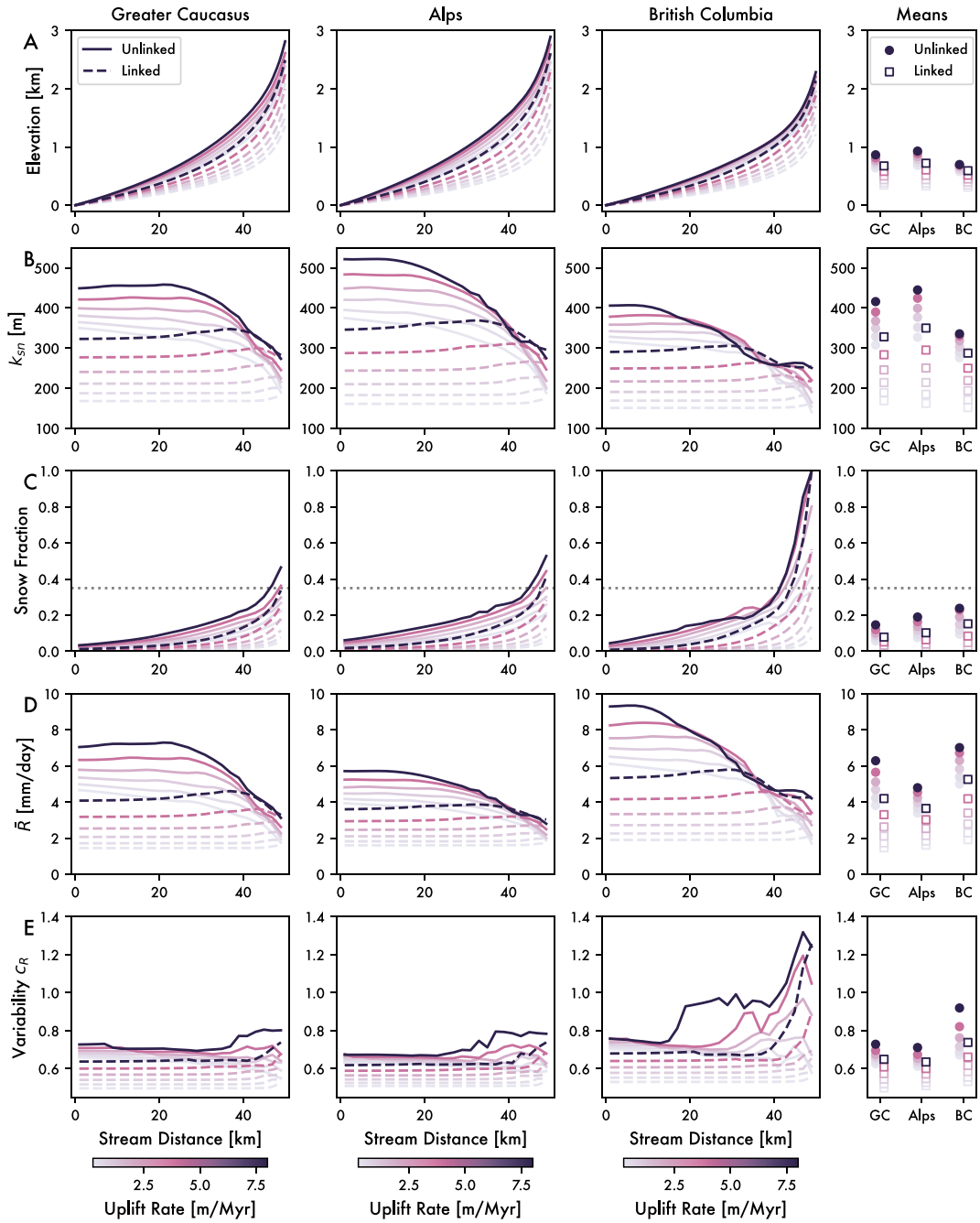

Figure 4. Steady state results for both unlinked (solid lines) and linked (dashed lines) models across the full range of uplift rates (0.25–8 mm/yr) for three regional cases (left column—Greater Caucasus, middle column—Alps, right column—British Columbia). The fourth column shows mean values of each quantity within the row for all three locations. Lines are colored by uplift rate. Rows show how (a) elevation, (b) mean k_{sn} within bins, (c) snowmelt within bins, (d) mean daily runoff within bins, and (e) runoff variability within bins vary as a function of stream distance. Note that these values represent the final 40 timesteps (representing 200,000 years of model time). This time-averaging was done because the individual timesteps show significant variability between output timesteps.

The dynamics of individual runs are decidedly complex despite them being 1D models. In the sections below, much of the behavior of individual model runs is not discussed in detail because we focus on general behavior. Outputs of all models are available in Forte and Rossi (2024a), along with summary plots of all model runs. Codes to interpret and interrogate the model results are available in Forte (2024).

5.1. Model Behavior Across Regional Cases

Comparison of the regional cases provides important insights into the behavior of spatial-STIM. Figure 4 shows the steady state results for three cases inspired by the modern hydroclimate of the Greater Caucasus, Alps, and British Columbia. Model results are shown for both linked and unlinked runoff parameters, a bin size of 2 km, a river length of 50 km, and uplift rates spanning from 0.25 to 8 mm/yr. Note that we refer to these results as reflecting "steady state," even though the majority of the model runs never truly reach steady state in the sense of invariant properties along the river profile. In detail, several behaviors can be gleaned from these comparisons. First, for all unlinked scenarios, there is a distinct upstream decrease in channel steepness. In contrast, channel steepness occupies a much smaller range of values for linked scenarios (Figure 4b). As a spatial gradient in k_{sn} effectively suggests a different true concavity than the imposed reference concavity, this result implies that, especially for the unlinked scenarios, the concavity of river profiles can substantially deviate from the 0.5 reference value used to calculate k_{sn}, a point we return to in the discussion. Second, upstream decreases in channel steepness (and thus local relief) are associated with decreases in mean runoff in those high elevation bins (Figure 4d) as should be expected from the imposed empirical relationships (e.g., Figure 2). Daily runoff variability also decreases upstream in line with increases in SF, though most of the longitudinal profiles generally remain below the snowmelt-dominated regime (Figure 4c). Third, Figure 4 reveals important differences between regional cases as a function of uplift rate. For example, despite the highest uplift rate being 32X the lowest uplift rate, the steady state river profiles for the unlinked British Columbia region are remarkably similar across the full range of rock uplift rates (Figure 4a), likely related to the higher SF (Figure 4c), mean runoff (Figure 4d), and lower variability (Figure 4e) of these model runs.

One main hypothesis of this study (Figure 1b) envisioned periods of time or locations in which the snowmelt-dominated regime (i.e., high mean runoff and low runoff variability) can substantially modify the sensitivity of channel steepness to increases in rock uplift rates. While motivated by three landscapes (and hydroclimatic rulesets) that might sample across this transition, only British Columbia achieves enough total relief to even begin to sample this part of parameter space (Figure 4c). For the other two rulesets, model runs rarely exceed the SF of 0.35 (Figure 4c), consistent with the empirical data from WaterGAP3 (Figure 2d). As a test of internal consistency, we also checked the mean runoffs and shape parameters for each bin across the full range of uplifts at all timesteps for the Greater Caucasus unlinked model run. The majority of bins stay within empirical ranges without any formal restriction to this range (Figure S2 in Supporting Information S1). This suggests that our new model is not extrapolating to unrealistic portions of parameter space during the transient evolution of these river longitudinal profiles.

When generalizing across all model runs in Figure 4, two main results emerge: (a) Differences in the steady state form of river profiles induced by different hydroclimatic forcings are relatively modest for a given rock uplift rate (Figure 4a); (b) Whether the recurrence interval of runoff events in spatial bins are linked or unlinked is more significant, especially when rock uplift rates are low (Figures 4a and 4b). Examining the mean values of metrics (far right column in Figure 4) highlights that differences among regional rulesets for a given set of model parameters (i.e., linked vs. unlinked, rock uplift rate) generally span a smaller range within a given region than the larger contrast between linked and unlinked scenarios. Because of this, we focus our initial analysis of transient model dynamics on the assumption of linked versus unlinked runoff events.

5.2. Explaining Differences Between Unlinked Versus Linked Scenarios

We use the contrast between the Greater Caucasus unlinked recurrence interval of runoff events scenario with a 1 mm/yr uplift rate (GC1U) and its linked equivalent (GC1L) to help unpack model dynamics. As the longitudinal profile evolves toward steady state, a transient slope-break knickpoint migrates upstream (e.g., Figure 3), much like in other stream-power based models of river incision (e.g., Crosby & Whipple, 2006; Rosenbloom & Anderson, 1994). However, the key novelty to our model is that runoff statistics vary both in space and in time. For both the unlinked and linked scenarios, we identified a time when the knickpoint had obtained a similar relative upstream position (Figures 3a and 3b; 1 Ma for unlinked; 0.63 Ma for linked). Figures 3c–3f show the runoff parameters for every bin in the profile at that time. On these plots, we show the spatially averaged values for the shape parameter and mean runoff. We also show the median values of those parameters for a Monte Carlo simulation (500 trials) of randomly sampled, 100-year long discharge records using the orographic rules for this timestep. Both the unlinked and linked scenarios show that mean runoff is similar whether averaging across bins or routing runoff down the profile (i.e., the Monte Carlo estimates). In contrast, a persistent feature of unlinked scenarios is that the variability

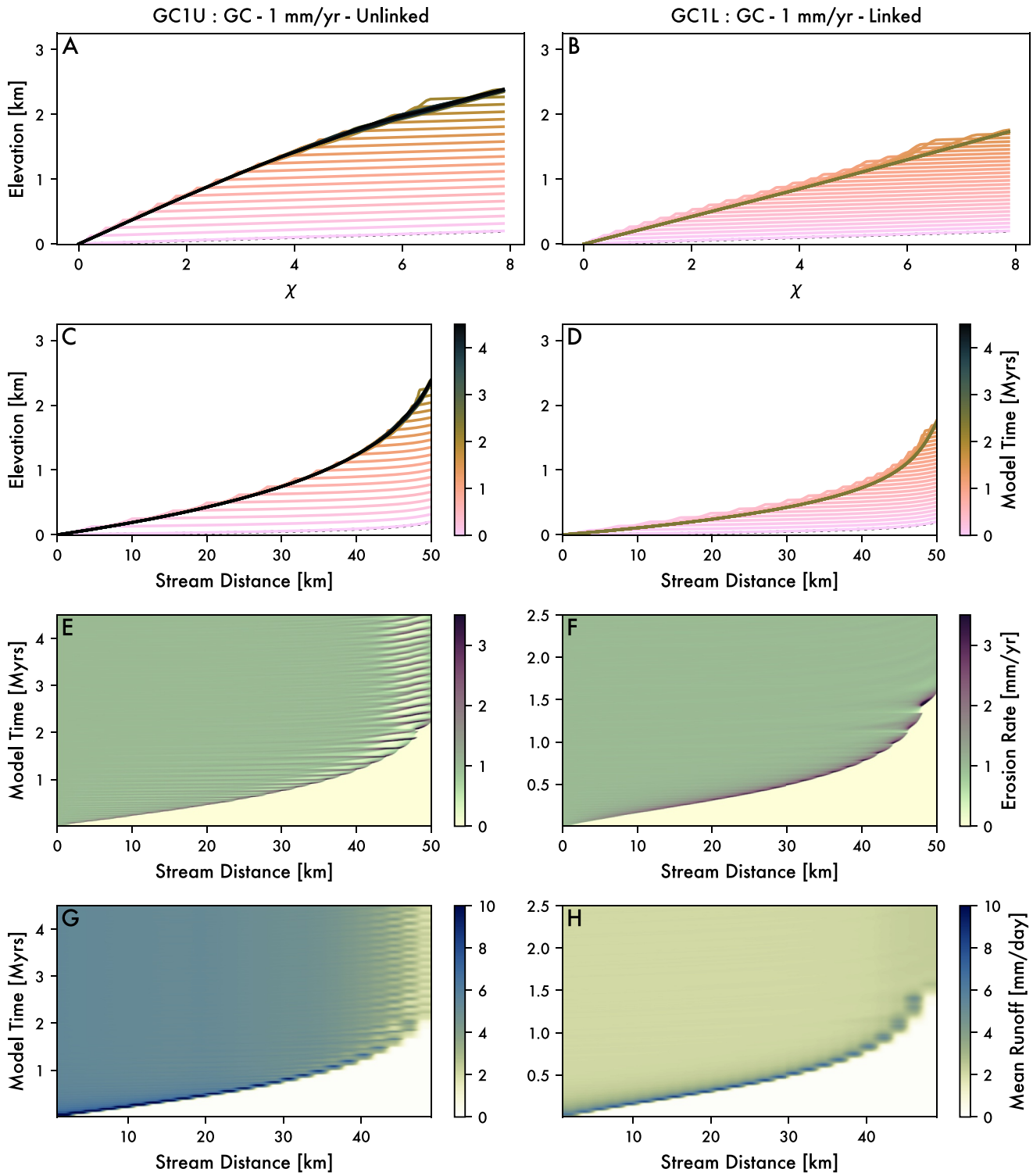

Figure 5. Representative stream profile evolution for an unlinked (left column) versus linked model (right column) for the Greater Caucasus uplifting at 1 mm/yr. (a) χ-elevation for model GC1U through time showing 40 equally spaced time slices. (b) Same as in A but for GC1L. (c) Stream profile for model GC1U through time for the same 40 equally spaced time slices as in panel (a). (d) Same as in C but for GC1L. (e) Average erosion rate between outputs along the profile for model GC1U for all output time slices. (f) Same as in E but for GC1L. (g) Mean runoff within bins for all output time slices for model GC1U. (h) Same as in G but for model GC1L.

of routed discharge is significantly lower (i.e., larger shape parameter) than the corresponding averages of bins would suggest (Figures 3c and 3e), a behavior not observed in the linked scenarios (Figures 3d and 3f).

To expand beyond one moment in time, Figure 5 shows the contrast in model runs as a function of χ and stream distance for the Greater Caucasus hydroclimatic ruleset (e.g., Figures 2c and 2d). The temporal evolution of χ-elevation plots (Figures 5a and 5b) and longitudinal profiles (Figures 5c and 5d) reiterate that unlinking the runoff statistics as a function of profile position reduces the efficiency of erosion (i.e., generates steeper steady profiles). However, while the overall erosional efficiency is lower, the unlinked hydroclimatic parameters actually produce more significant (and temporally isolated) pulses in erosion during the transient evolution of the profile (contrast stripes in Figure 5e with 5f) and greater mean runoffs (more blue in Figure 5g than 5h). Unlinked cases also generally take longer to reach a quasi-steady state (Figure 5). Here specifically we consider these profiles to be in a quasi-steady state in the sense that the elevations (and associated parameters, e.g., relief, etc.) never reach a truly static value, but effectively oscillate around an average value. We briefly offer our explanation for this apparent disconnect between long-term model behavior and what would be observed during a single snapshot of erosion along the river profile.

Interpreting the dynamics in spatial-STIM requires understanding the frequency of exceedance of erosional thresholds in the model (Figure 6). In our numerical experiments this threshold is held constant for all model runs. For both the linked and unlinked scenarios, areas above knickpoints rarely exceed the threshold for erosion and are thus passively uplifted until a knickpoint passes. The knickpoint itself focuses threshold exceedances to an area just below where channels are steepest (red areas along profile in Figures 6a and 6b). This hotspot in threshold exceedance is localized near the knickpoint for the linked case and persists in downstream reaches for the unlinked case. Because the knickpoint is migrating upstream, cumulative threshold exceedances as a function of stream position are relatively smooth when averaged over the long-term (Figures 6c and 6d) with an average that stabilizes to a single value (Figures 6e and 6f). Threshold exceedance frequencies are generally higher in the unlinked case (Figures 6e–6h). In addition, local erosion rates can get much higher in the unlinked case (e.g., Figures 5e, 5f, 6g, and 6h). Taken alone, these observations might suggest a more efficient hydroclimate in the unlinked case. However, both river profiles are approaching a quasi-steady state suggesting that river profiles needed to adjust to more frequent temporal exceedances to overcome the spatial heterogeneity in runoff generation. Specifically, the unlinked case inhibits the "benefit" of water flowing from upstream. Higher probabilities of exceedance are needed in upstream reaches to balance rock uplift, which are accommodated by steepening, because rare runoff events are not synchronous along the river profile. These dynamics result in a negative upstream trend in cumulative exceedance (Figure 6c) that is not observed in the linked case (Figure 6d). The linked scenarios are thus able to maintain lower relief at lower mean discharges because of the spatial autocorrelation of events in a river basin. The assumption for how runoff events accumulate downstream appears to be an under-appreciated governor of model dynamics, that is perhaps more important than the orographic rules for hydroclimate we use.

Finally, an additional difference between unlinked and linked cases is the perpetuation of some amount of dynamic instability in the unlinked models. This can be seen in comparisons of temporal and spatial variations in erosion rate (contrast Figure 5e with Figure 5f) and the frequency of exceedance of erosion thresholds (contrast Figure 6a with Figure 6b) between the unlinked and linked models. Even after the main transient knickpoint has propagated completely through the landscape, there are quasi-periodic erosional "events" that continue to impact the unlinked models, which lead to small-scale variations in profile topography. To understand this behavior, it is worth considering the dynamics at play after the profile reaches its quasi-steady form. In both cases, not every daily event will erode. In the linked cases, whether a given event will erode (i.e., whether it exceeds the erosion threshold) will be tend to be spatially uniform as the whole profile has nearly adjusted to the same threshold condition. In contrast, for unlinked cases, events that exceed the erosion threshold will occur only in a portion of the profile (i.e., the bin where the event occurs and possibly in bins downstream). This effectively generates small knickpoints in the profile that subsequently propagate upstream. The local change in steepness will similarly modify the critical discharge necessary to exceed the erosion threshold, further accentuating this new perturbation. Because there is no damping mechanism for these small perturbations in the unlinked scenarios, the river profile is inherently less stable.

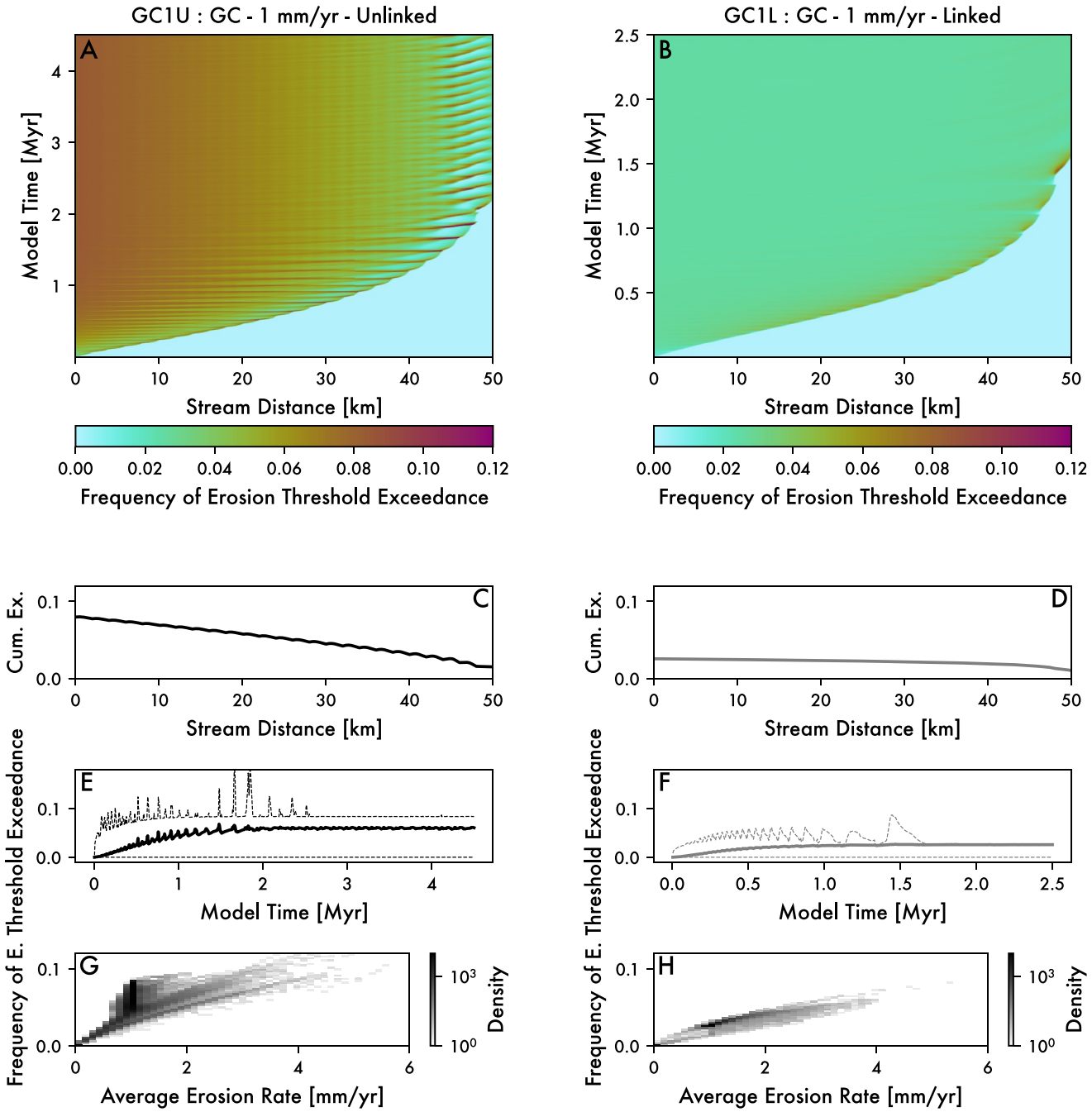

Figure 6. Frequency of exceedance of the erosion threshold between output timesteps in an unlinked (left column) versus linked (right column) scenarios, specifically for the Greater Caucasus uplifting at 1 mm/yr. (a) Plot of frequency of exceedance as a function of profile distance (x) and model time (y) for the unlinked GC1U model. The area of consistently higher frequency of exceedance tracks the movement of the knickpoint through the profile. (b) Same as in panel (a) but for the linked GC1L model. (c) Cumulative frequency of exceedance of the erosion threshold across the entire model run as a function of stream distance for unlinked model GC1U. (d) Same as in C but for linked model GC1L. (e) Mean (solid lines) and maximum and minimum (dashed lines) frequency of erosion threshold exceedance through time for the GC1U model. (f) Same as in E, but for the linked model GC1L. (g) Individual frequencies of exceedance of erosion threshold at a specific node compared to the average erosion rate of that node for all time steps for unlinked model GC1U. (h) Same as in panel (g), but for linked model GC1L.

5.3. Sensitivity of Spatial-STIM to Other Elements of Model Structure

While the most significant difference between model outcomes is tied to whether the runoff distributions are linked or unlinked along the river profile, other structural elements of the model are also important to model dynamics. Specifically, we interrogate how the three new model parameters added to spatial-STIM (bin size,

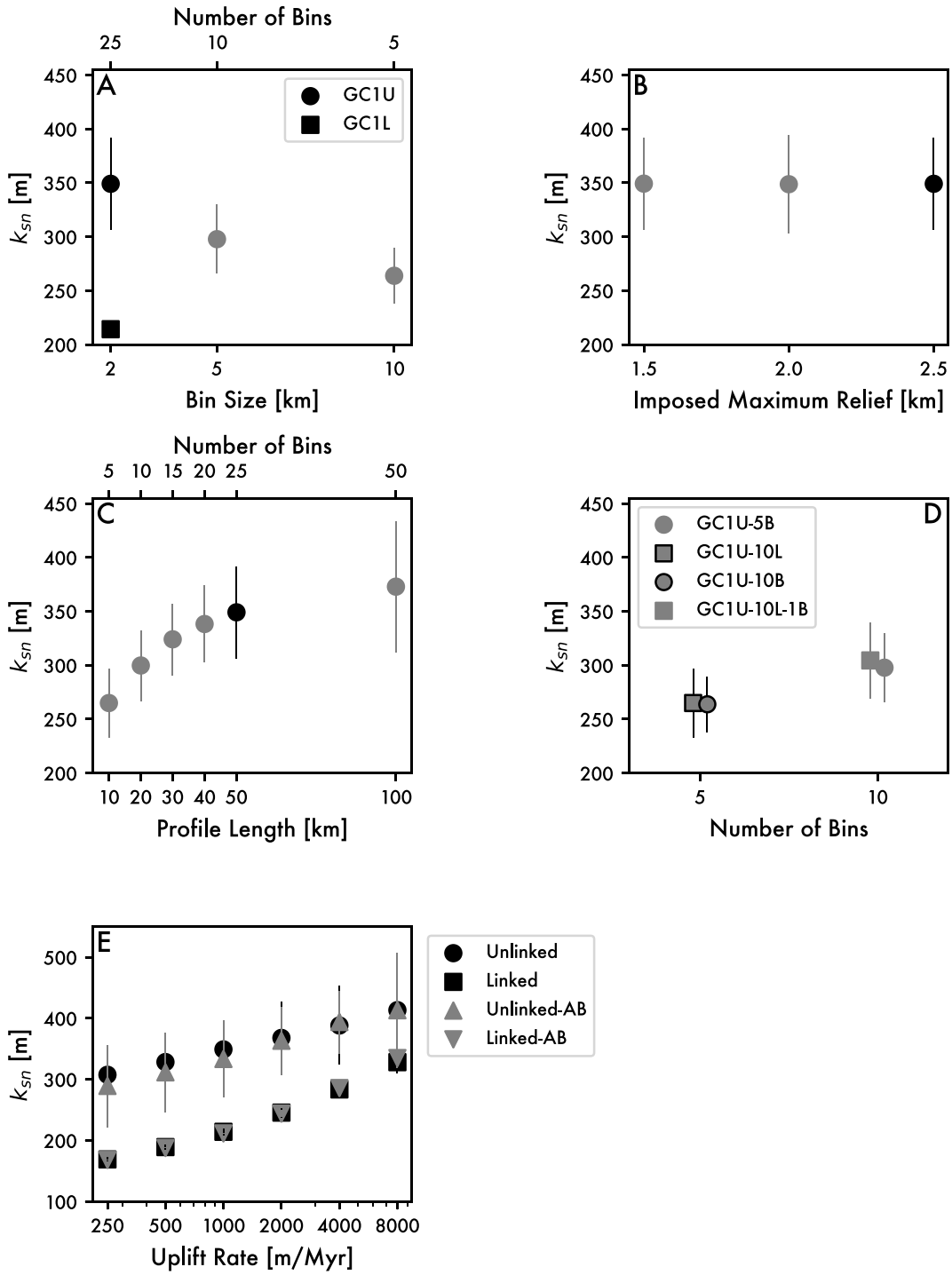

Figure 7. Summary of sensitivity experiments. Black circles and squares indicate results of reference experiments shown previously, and gray symbols indicate results from sensitivity test. Triangles are used to show results using area binning. In panels (a–d), uplift rate is 1 mm/yr and the Greater Caucasus hydroclimatic ruleset is used. (a) Sensitivity to bin size used for runoff parameters. See Figure S3 in Supporting Information S1 for steady-state output of relevant models. (b) Sensitivity to the imposed maximum relief. See Figure S3 in Supporting Information S1 for steady-state output of relevant models. (c) Sensitivity to the profile length. See Figure S3 in Supporting Information S1 for steady-state output of relevant models. Note that for all of these models, the bin size is kept at 2 km, so different profile lengths imply a different number of bins. (d) Sensitivity to the number of bins, comparing models that are either 50 km (squares—GC1U-5B, GC1U-10B) or 10 km (circles—GC1U-10L, GC1U-10L-1B) long. (e) Sensitivity to equal river length binning (black circles and squares) versus equal area binning (ab—gray triangles) across the full range of uplift rates used in numerical experiments.

maximum local relief, profile length) and one derived parameter (number of bins) influence model behavior (Figure 7). This latter parameter encodes the ratio between the size of the system (profile length) and the scale over which changes in hydroclimatic parameters are represented (bin size). We also test the importance of how the profile is binned, namely when uniformly subdivided by river length versus contributing drainage area.

For all sensitivity experiments, we use the Greater Caucasus hydroclimatic parameters and generally use rock uplift rates of 1 mm/yr, except for experiments testing the way the profile was discretized (Figure 7e). In all cases, the steady-state channel steepness is what is being compared. Reference conditions (black squares and circles) assume 50 km river lengths, bin sizes of 2 km, and a maximum imposed relief of 2.5 km. For unlinked scenarios, the sensitivity of k_{sn} to bin size is substantial (Figure 7a, Figure S3 in Supporting Information S1). A 5X increase in bin size corresponds to ∼33% reduction in k_{sn}. Increasing the size of bins both decreases the granularity with which orographic gradients in hydroclimatic parameters are represented as well as increases the degree of spatial autocorrelation. To the latter point, we also plot the linked case to show that the effect of increasing bin size is approaching the k_{sn} values observed when the events are linked over the entire river profile. For the majority of model runs, we consider bins of equal river distance. Because of the power-law scaling between distance and drainage area, this implies that the contributing area of each bin is not the same. As such, we test a set of both linked and unlinked model runs that use bins of equal drainage area (Figure 7e). When the number of bins is the same, the results for linked models are identical to the distance bin models. For unlinked cases, the area and distance bin results are different, but overlap within uncertainty. The sensitivity of k_{sn} to maximum local relief is near zero (Figure 7b, Figure S3 in Supporting Information S1). It is worth noting that this threshold in maximum local relief was set to prevent extrapolating our runoff parameter relationships to unrealistic values. The insensitivity of channel steepness to this maximum local relief gives us confidence our model interpretations are not unduly sensitive to this threshold parameter. We suspect that if the maximum relief was set to unrealistically low or high values, it would begin to influence model results. For unlinked scenarios, the sensitivity of k_{sn} to profile length, and thus system scale, is substantial (Figure 7c, Figure S3 in Supporting Information S1). A 10X increase in profile length corresponds to ∼50% increase in k_{sn}. Increasing the length of profiles, while holding bin size constant, increases the granularity with which orographic gradients in hydroclimatic parameters are represented by creating more bins for a given elevation gradient. Because both bin size and profile length impact the granularity of orographic gradients in runoff parameters, we also did a test where we changed the length of the profiles (10 and 50 km) for different bin numbers (Figure 7d). Systems of different lengths had similar values for k_{sn} as long the number of bins was the same. More bins, and thus finer resolving power of gradients in runoff parameters, led to slight increases in steady k_{sn}. For example, a 2X increase in bin number led to ∼15% increase in k_{sn}, albeit within uncertainty of estimated values.

6. Discussion

Adding complexity to geomorphic transport laws like stream power is only useful to the degree that a new model is able to: (a) Be implemented over the spatiotemporal scales of interest; (b) Capture dynamics that cannot otherwise be simulated; and (c) Improve the ability to calibrate models and test hypotheses with empirical data. Given that stream power is one of the most widely used erosion laws in landscape evolution studies, we critically evaluate the results from our model analysis using spatial-STIM. First, we first compare spatial-STIM model results to its stream-power based predecessors. Second, we articulate the scenarios where and when spatial-STIM has the potential to provide more physically based and empirically constrained predictions. Third, we discuss the limitations of this new 1-D model, along with ideas for future research directions.

6.1. Spatial-STIM and Its Predecessors

One useful lens through which to consider model results is in how spatial-STIM predictions compare to other 1D models built on stream power (Howard, 1994; Whipple & Tucker, 1999). We focus on three important metrics to evaluate how our new model compares to its predecessors—namely the steady state channel steepness, the steady state concavity, and the response times to steady state.

6.1.1. Steady State Channel Steepness

Figure 8 shows the steady state relationships between channel steepness and erosion rates for our regional cases using both linked and unlinked parameters. We plot results both in terms of k_{sn} and k_{snQ} using a reference channel

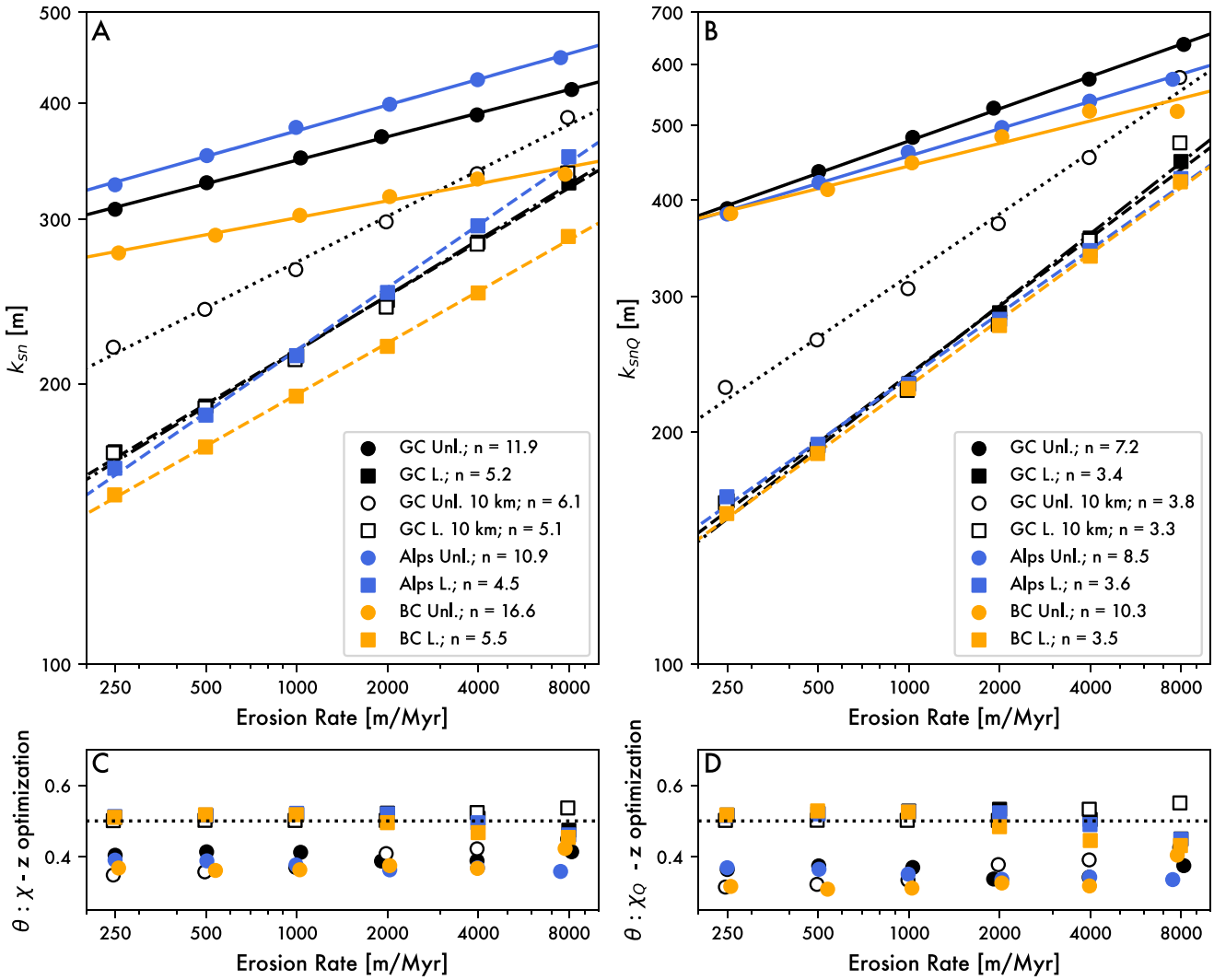

Figure 8. (a) Mean k_{sn} and erosion rate at quasi-steady state. Lines are power law fits to model results in a stream power context. Equivalent n values for each stream power relationship are shown in the legend. Note each point includes uncertainty as the standard error on the mean, but are generally are less than the width of the symbols. (b) Same as in A but calculating k_{snQ} sensu Adams et al. (2020), which uses precipitation as a proxy for runoff to calculate discharge. To accomplish this in our 1D model results (which do not formally calculate precipitation), we use empirical relationships between runoff and precipitation from WaterGAP3 for each region to estimate precipitation based on the modeled runoff. We compare the results of calculating k_{snQ} directly from runoff in Figure S4 in Supporting Information S1, but ultimately the differences are subtle. (c) Best fit concavity (θ) for models using drainage area. Dotted line is the expected concavity of 0.5 given the input values in the model (d) Best fit concavity for models using precipitation weighted drainage area sensu Leonard et al. (2023b).

concavity of 0.5 (see Section 6.1.2 for discussion on patterns in concavity). For any given scenario, all model results are well approximated by a power law, similar to predictions from simple stream power (e.g., Equation 8). In general, power law fits of channel steepness show strongly sublinear behavior and imply stream power values of n of 4.5–5.5 for linked scenarios and 6.1–16.6 for unlinked scenarios (Figure 8a). That individual scenarios imply different values for K and n should be expected because these stream power parameters encode details of both climate and rock properties (e.g., Kirby & Whipple, 2012; Whipple et al., 2022), the former of which we are explicitly varying in each different scenario. However, the wide range and large magnitudes of n are a bit more surprising and could be interpreted in empirical data sets as channel steepness thresholds (Hilley et al., 2019). Consistent with other stochastic-threshold models of river incision (see Lague, 2014), effective values of n are expected to correlate with the shape parameter of the runoff distribution (Figure 9a), though our results are not entirely analogous. The relationship between the shape parameter of the runoff distribution and n largely emerges from the unlinked cases in our model results. For the linked cases, which are more analogous to the Lague et al. (2005) model, similar runoff variabilities produce a more modest range of values for n. Our data does largely

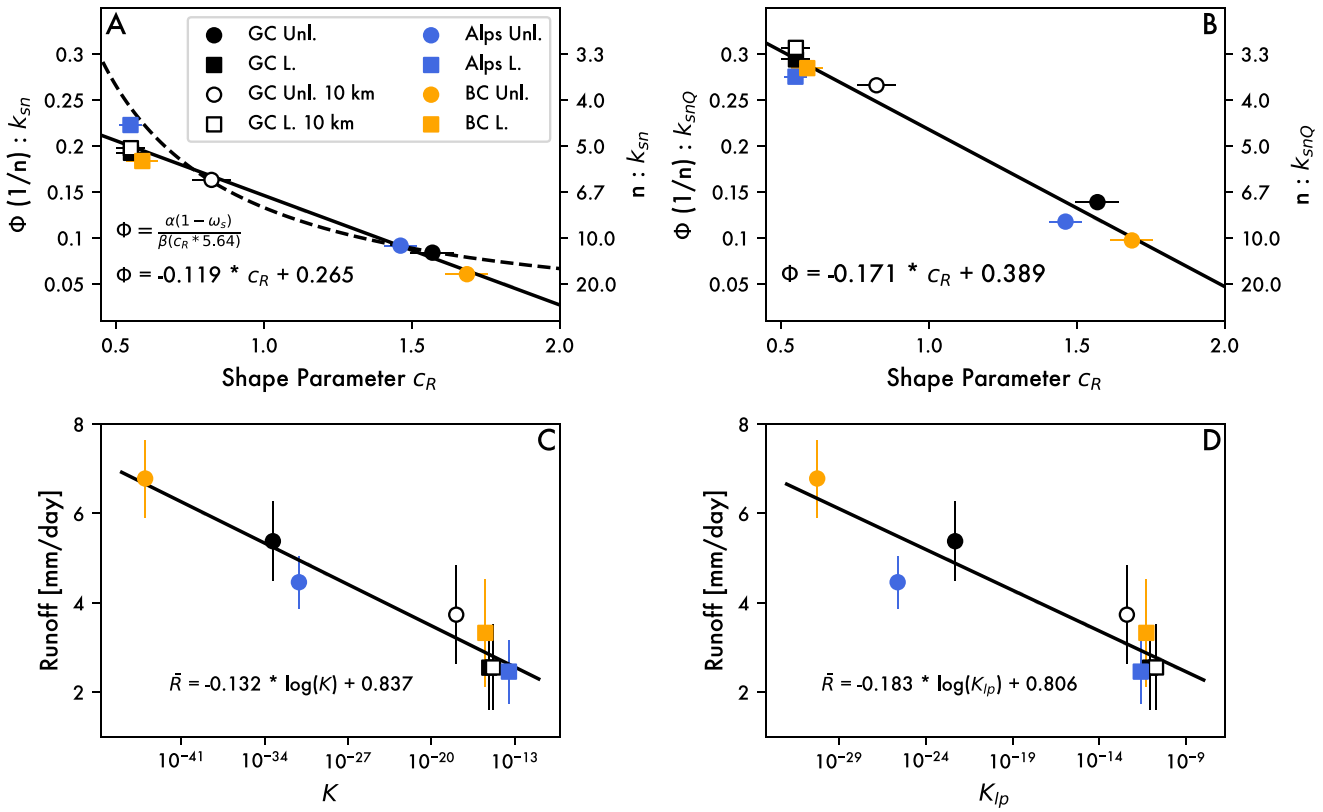

Figure 9. (a) Mean shape parameter across models for a given scenario compared to 1/*n* from fits in Figure 8a. Solid line is linear fit through the data. Dashed line is expected relationship from Lague et al. (2005) after converting Weibull shape parameters to inverse gamma ones using the relationship in Rossi et al. (2016). (b) Mean variability across models for a given scenario compared to 1/*n* from fits in Figure 8b, that is, when fitting a relationship between k_{snQ} and erosion rate. (c) Mean runoff across models for a given scenario compared to *K* from fits in Figure 8a. (d) Mean runoff across models for a given scenario compared to K_{lp} from fit in Figure 8b. Symbol style is shared across all plots.

overlap with the predicted relationship between the shape parameter and 1/*n* from Lague et al. (2005) assuming a case where erosion thresholds are large with respect to erosion rates (Figure 9a), but is slightly better explained by a simple linear relationship. Intriguingly, a negative correlation between *K* and mean runoff emerges from the spatially varying hydroclimatic rules used to evolve the profiles (Figure 9c).

We also present the corresponding topography - erosion rate relationships using an alternative calculation of channel steepness, k_{snQ}. We do this to explore whether normalizing our calculations by spatial gradients in runoff can help collapse model results onto a single functional form, thus following up on the recent empirical successes of using k_{snQ} (Adams et al., 2020; Leonard et al., 2023a, 2023b). Using k_{snQ} instead of k_{sn} does reduce the overall range of stream power values of *n* to ∼3.3–3.6 for linked cases and ∼3.8–10.3 for unlinked cases (Figure 8b). Within either linked or unlinked models, this also collapses the range for individual regions, though much more so for the linked than unlinked scenarios. Despite these modest improvements in using k_{snQ}, this modified form of channel steepness does not collapse model results onto a single relationship as might otherwise be expected for model runs with the same underlying rock properties (i.e., same values for k_e, τ_c, and k_w). The point is emphasized further in the persistence of trends between shape parameter and *n* (Figure 9b) and runoff and K_{lp} (Figure 9d) for values from the k_{snQ}-*E* relationships (Figure 8b). The overall relationships between stream power parameters and the two different calculations of channel steepness are quite similar, though they differ in detail as the rank order of values change between k_{sn} (Figures 9a and 9c) and k_{snQ} (Figures 9b and 9d).

6.1.2. Steady State Concavity

Other 1D river incision models show that steady state concavity is differentially sensitive to orographic gradients in precipitation as a function of rock uplift rate (Roe et al., 2003), though they typically fall within the range of expected values between 0.4 and 0.6 (Whipple et al., 2022). As such, we consider best-fit concavities both using

drainage area (Figure 8c) and precipitation-weighted drainage area (Figure 8d). For each model run, we determine the best-fit concavity by using the linear relationship between χ-elevation or χ_Q-elevation (sensu Leonard et al., 2023b). All model runs use a ratio of the area exponent, m, to the slope exponent, n, of 0.5. Deviations from this value thus indicate concavity anomalies induced by differences in how runoff is generated in the model. The range of concavities spans from ~0.3 to 0.5. Importantly, unlinked scenarios consistently develop profiles with concavities <0.5, consistent with the spatial pattern of k_{sn} observed in the steady state profiles of those models (e.g., Figure 4b). In contrast, linked scenarios consistently develop profiles with concavities ~0.5. For linked scenarios, the largest negative anomalies (i.e., negative deviations from 0.5) occur at the lowest uplift rates, which then approach the expected concavity of 0.5 at higher rock uplift rates. However, examination of along profile patterns in k_{sn} for these high uplift rate, linked models (e.g., Figure 4b) suggest that the apparent match of concavities masks persistent deviations in k_{sn} in the upper reaches of the profile. Because there is a tradeoff between the relative roles of mean runoff and daily runoff variability on erodibility, numerical models like spatial-STIM are needed to identify how sensitive concavity is to rock uplift rates. For a given set of hydroclimatic parameters, concavity can vary by ~0.1. We also note that precipitation-weighted concavity for unlinked models (Figure 8d) shows more sensitivity to rock uplift rates than conventional calculations of concavity. This is the opposite of the effect described in Leonard et al. (2023b) where these authors showed that precipitation-weighted concavity reduces the dynamic range of values observed in central Andean drainages. Based on this, we suggest that systematic changes in channel concavity with rock uplift rates may provide important insights into the importance of orographic effects on runoff parameters. In particular, we hypothesize that the relative scale of runoff generating events to the size of a watershed may be imprinted in the concavity. We return to this idea in Section 6.2.

6.1.3. Transient Response Timescales

Stream power predictions of steady state morphology are non-unique (Gasparini & Brandon, 2011). By instead targeting the functional relationship between channel steepness and erosion rate for a given set of environmental conditions (e.g., rock properties, climatic setting), stream power predictions are more discriminating, but are still non-unique. For example, there is always a K and n - or K_{lp} and n - pair that can describe the expected steady state topography produced by our model outputs in each of the simulated scenarios (Figures 8 and 9). As such, we consider here whether differences in model dynamics are observed in the transient response of the 1D river profiles. To assess this, we compared the response times to steady state for both spatial-STIM and simple stream power. We calculated the analytical solution to stream power using the equations in Whipple (2001). Using the Hack parameters from model initialization (Equation 21), we can derive the analytical solution for response times using the fit values for K and n in each model scenario. To do this, we first back-calculate the initial rock uplift rates that correspond to the initial k_{sn} of 25 m used in all model runs. We then calculate the fractional change in rock uplift rates and apply the equations in Whipple (2001) to calculate a response time. For comparison to spatial-STIM, we have to also define steady state in our numerical runs. We define the time to steady state as the time it takes for the absolute value of the difference between maximum elevations of the profiles to fall below 10% of the amount of uplift per output timestep. This was used to account for the continual time variation in profiles for unlinked cases. Figure 10 summarizes these calculations and includes direct comparison between spatial-STIM and the analytical solutions for stream power (Figure 10c). Response times for spatial-STIM plot very close to the 1:1 line, suggesting broad agreement. Importantly, while simple stream power model can reproduce the transient dynamics of spatial-STIM, the values of K and n cannot be derived from first principles. In other words, the values for these parameters are not readily inferred from known differences in modern estimates of mean runoff and daily runoff variability used in our three regional scenarios.

6.1.4. Comparison of Spatial-STIM and STIM

Some of the behaviors we observe in our results are expected from prior applications of STIM (DiBiase & Whipple, 2011; Lague, 2014; Lague et al., 2005), namely that Φ is directly related to the shape parameter of the streamflow distribution (Figure 9a). Furthermore, the general expectation that increasing relief and elevation leads to commensurate increases in mean runoff, SF, and the shape parameter of runoff distributions can be partially represented in zero-dimensional versions of STIM by altering the scaling exponent that relates drainage area to discharge. In fact, one key advantage of prior applications of STIM is that streamflow distributions can be linked to ecohydrological models driven by rainfall (e.g., Botter et al., 2009) or snowmelt (e.g., Schaefli

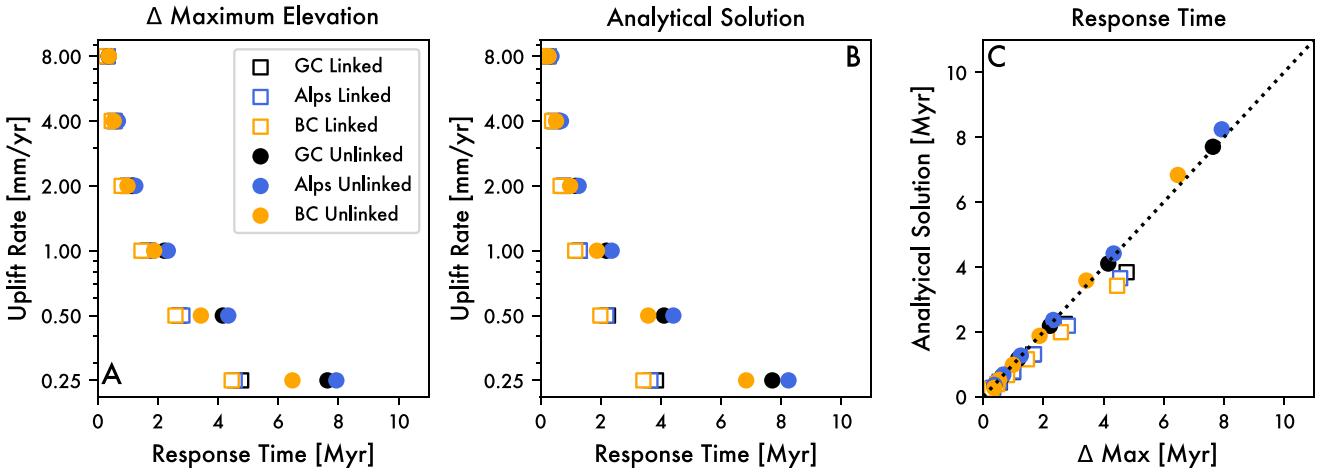

Figure 10. Comparison of analytical steady state (stream power incision model) to empirical steady state (stochastic-threshold incision models). (a) Estimated time to steady-state from model initiation using the change in maximum elevation between saved timesteps and defining steady-state as when the absolute value of this metric drops below 10% of the amount of uplift per output timestep. (b) Analytical solution for response times using estimates of K and n from Figure 8. The initial uplift rate for each model uses this K and n and the starting k_{sn} (25 m) to calculate the appropriate fractional change in uplift rate sensu Whipple (Whipple, 2001). (c) Comparison of the empirical and analytical response times.

et al., 2013). Under this theoretical framing, streamflow variability can then be derived from the characteristic timescale of runoff generating events, the hydrological response timescale, and the shape of the recession limb of the hydrograph (Deal et al., 2018). This physically based theory allows for the coupling of hydrology to bedrock river incision with a minimal set of parameters. However, at the mountain range scale, orographic effects can be substantial and runoff generation heterogeneous, making it difficult to couple ecohydrological models to bedrock river incision.

To begin to address this challenge, we adopted an empirical, rules-based approach to simulate how stochastic runoff coevolves with topography (Forte & Rossi, 2024b). By incorporating orographic patterns in mean runoff and daily runoff variability that may or may not be autocorrelated, spatial-STIM can predict profile evolution with upstream variations in topography (Figures 4a and 4b) and hydroclimate (Figures 4c–4e) that are not possible in spatially uniform variants of STIM. Importantly, predictions of relationships between k_{sn} and erosion rate differ between STIM and spatial-STIM (Figure 11, Figure S5 in Supporting Information S1). To aid comparison, we use the mean k_{sn} of the steady state profile and estimates of mean runoff and daily runoff variability to contrast spatial-STIM with its zero-dimensional equivalent using Equation 18. This is akin to treating the model results as a natural watershed, with which we might attempt to characterize using STIM. Such comparisons highlight that erosion rates within spatial-STIM and those predicted by STIM are different by between 0.5 and 1.5× (Figure 11a, Figures S6a and S6b in Supporting Information S1). The differences between STIM and spatial-STIM are more extreme for the unlinked cases than the linked ones. As catchments become smaller (and thus the degree of orographic variation within catchments becomes smaller), predictions of zero-dimensional STIM and spatial-STIM become more similar (e.g., note the 10-km long profile runs in Figure 11a). Similarly, if we use the mean runoff and variability of individual model runs to predict suites of k_{sn}-erosion rate relationships, we find relatively large differences in n between zero-dimensional STIM and spatial-STIM (Figure 11b, Figures S6c and S6d in Supporting Information S1). Spatial-STIM tends to be less linear (i.e., higher n) for linked models and more linear (i.e., lower n) for unlinked models (Figure 11d). This analysis highlights that when interpreting empirical k_{sn}-erosion rate relationships from cosmogenic erosion rates, one should be mindful of the potential presence of orographic gradients in relevant STIM parameters (i.e., mean runoff and variability), but also the spatial scale of runoff events (i.e., whether a linked or unlinked case is more appropriate). In scenarios where there appear to be orographic gradients within individual basins and/or that the scale of runoff individual events tend to be smaller than the basin itself, interpreting k_{sn}-erosion rate data with a zero-dimensional STIM model may make it difficult to relate the k_{sn}-erosion rate data to empirical constraints on runoff parameters.

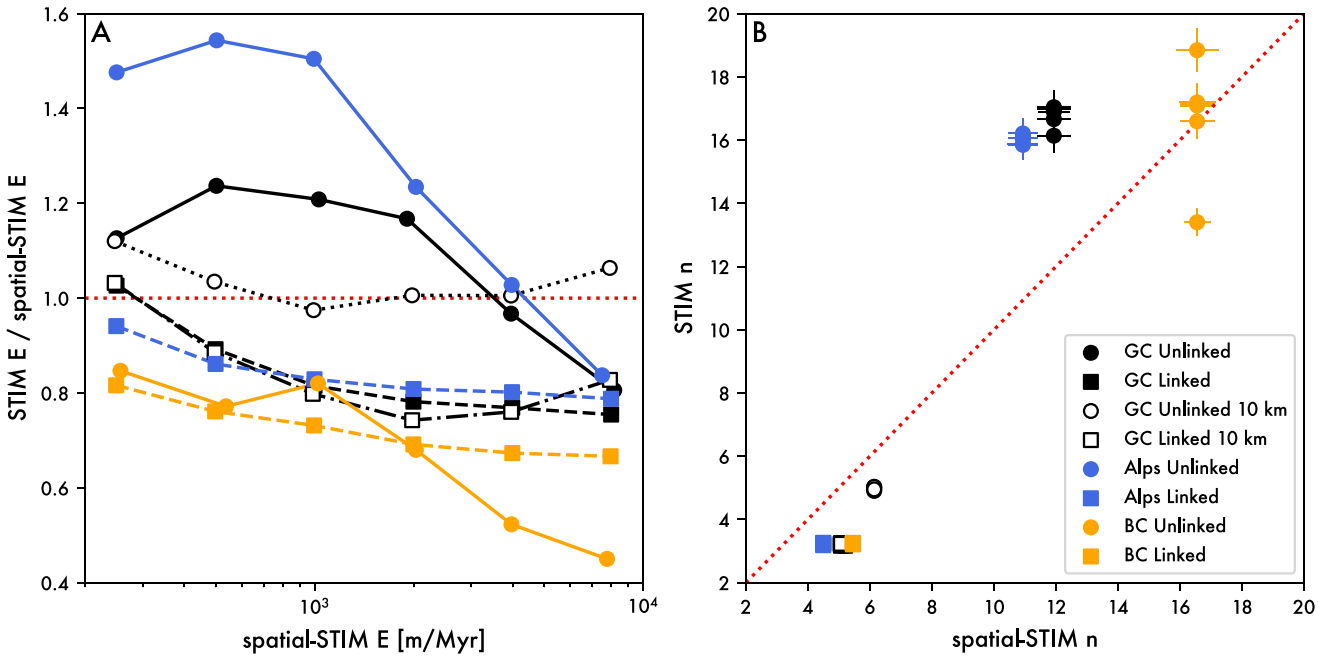

Figure 11. Comparison of zero-dimensional stochastic-threshold incision models (STIM) predictions and spatial-STIM results. (a) Ratio of erosion rates from two models as a function of spatial-STIM erosion rates. Direct comparison of values with uncertainty shown in Figure S5a in Supporting Information S1. (b) Comparison of power law exponent n for zero-dimension STIM and spatial-STIM. Note that for each model suite (i.e., a given regional hydroclimatic ruleset where bin are either linked or unlinked), there are six possible values of n predicted from zero-dimensional STIM. This is because each uplift rate generally produces a different catchment averaged runoff and variability and thus predicts a different k_{sn}-E relationship with a corresponding n value. Error bars represent uncertainty on the exponent from the fitting algorithm. Individual zero-dimensional STIM k_{sn}-E relationships are shown in Figure S5c in Supporting Information S1.

6.2. Why Use Spatial-STIM?

The stream power approximation for each scenario simulated in this study adequately explains both the steady state and transient response of river profiles. However, there are other reasons to favor using spatial-STIM for some applications. In particular, it provides insight into how process representation dictates model dynamics. Tethering process to the stochastic properties of runoff generation as function of relief development and spatial scale has potentially important implications on climate tectonic coupling.

6.2.1. Process Representation in Spatial-STIM

Any attempt to calibrate a 1D model of river incision is going to attempt to constrain free parameters using observational data. While most of our model parameters are fixed, we were able to produce a wide range of behaviors in spatial-STIM by simply including empirical patterns between mean runoff and daily runoff variability for three regional settings. Surprisingly, the details of hydroclimatic rules were less important than one new structural element to our model (i.e., the linking or unlinking of the recurrence interval of individual runoff events across bins) that essentially handles the spatial autocorrelation of runoff events. As an illustrative example, consider that we have good evidence for mixed populations of runoff generating events being sourced from snowmelt and rainfall-runoff in the Greater Caucasus (Forte et al., 2022). Using the same set of hydroclimatic rules, the K and n for linked and unlinked cases are very different. Attempting to fit stream power parameters to explain a mixture of the two endmembers would likely produce hybrid values of K and n that are not reflective of either runoff source or the expected behavior of the system (e.g., response times or the use of channel steepness to predict erosion rates). One could imagine that the differences between linked and unlinked models in terms of k_{sn}-erosion rate relationships (e.g., Figure 8a) reflect envelopes on possible k_{sn}-erosion rate data sets, and thus a wide array of K and n values (with K being in part of a function of n) that could be fit to the data. In all circumstances, the fit K and n would not be physically meaningful.

Because of how runoff processes are represented in spatial-STIM, our model analysis highlights that unlinked models are quite sensitive to event size (Figure 7a) and watershed size (Figure 7c). These findings place central

importance on understanding the hydroclimatic controls on the ratio of these two spatial scales (Figure 7d) if we want to understand the topographic response to BL fall. Empirical studies (e.g., Binnie et al., 2007; Cyr et al., 2010; DiBiase et al., 2010; Forte et al., 2022; Harkins et al., 2007; Miller et al., 2013; Olivetti et al., 2012; Ouimet et al., 2009; Rossi et al., 2017; Safran et al., 2005; Scherler et al., 2014) typically sample across a range of watershed sizes that may be interacting in complex ways with the characteristic scale of runoff generating events. Given this strong sensitivity to spatial scale, it is unclear how generalizable empirical estimates of K and n are when comparing across landscapes. While typical uncertainties associated with erosion thresholds (e.g., Shobe et al., 2018), rock erodibility (e.g., Yanites et al., 2017), channel width scaling (e.g., Gallen & Fernández-Blanco, 2021), and sediment flux dynamics (e.g., Whipple & Tucker, 2002) still remain (and were not explored in this analysis), we argue from our simulations that we may not be accounting even for the most important aspects of climate in current models of bedrock river incision. As such, there is a need for providing mechanistic explanations of the "linked" versus "unlinked" scenarios.

6.2.2. Physical Interpretations of Unlinked Versus Linked Scenarios

Given the central importance of whether the recurrence times of daily runoff are synchronous along the river profile (i.e., "linked" in the parlance of the model), there is a need to provide physical interpretations to this new structural element in the model. We argue that linking or unlinking runoff statistics spatially embeds a variety of physically distinct mechanisms. The first broad class of interpretations of linking the recurrence times of daily runoff is that it, in part, it captures the spatial scale of rainfall events—particularly, the contrast between synoptic scale rainfall versus convective rainfall. While actual rainfall fields vary continuously, our bin-based treatment facilitates representing orographic gradients in daily rainfall that vary in magnitude but where the relative frequency is uniform (or not in the "unlinked" scenarios). Whether recurrence times are uniform at the event scale is an important consideration. In some cases, precipitation patterns during individual storms mirror long-term means (e.g., Garvert et al., 2007; Minder et al., 2008; Roe, 2005). In contrast, there is also deep literature documenting how event-scale gradients in precipitation properties are more sensitive to finer-scale topography leading to more complex outcomes (e.g., Cosma et al., 2002; Marra et al., 2022). To some extent, spatial-STIM can capture some of this nuance. Even the linked scenarios can develop significant complications in spatial patterns in runoff when lower relief areas persist upstream, leading to a relatively lower magnitude of runoff events. Nevertheless, the linked and unlinked scenarios reflect not only the atmospheric forcing but also how the hydrologic response self-organizes in the landscape as function of topography.

The second broad class of mechanistic interpretations of whether runoff events are spatially linked lies in the assumed hydrology that converts precipitation events into daily runoff distributions. At even the simplest level, this probabilistic transformation is nontrivial (e.g., Rossi et al., 2016) such that a naïve correspondence between runoff generating events and the spatial characteristics of precipitation events becomes problematic. Land surface properties like vegetation (Deal et al., 2018), soil thickness (Rossi et al., 2020), among others, may plausibly co-evolve with topography in ways that can partition the landscape into domains with distinctively different rainfall runoff statistics. Furthermore, we showed in our companion paper (Forte & Rossi, 2024b) that the spatial extent of snowmelt dominated runoff events tends to dominate the far right tail of runoff distributions, especially at higher intensity thresholds. While our treatment only provides a crude representation of the endmember cases of linked versus unlinked scenarios, it provides a useful baseline for the range of outcomes for a given hydroclimatic ruleset. From the perspective of steady state relationships between channel steepness and erosion rates, reality likely lies somewhere in between the linked and unlinked scenarios, producing a large number of potential K—n pairs that can be plausibly produced for even a simple hydroclimatic ruleset. More attention to understanding and characterizing how the statistics of runoff might be spatially autocorrelated via a variety of physical mechanisms is a potentially fruitful, and important, future research direction.

6.2.3. Isolating the Effect of Snowmelt

While the snowmelt transition was in part our initial target of model development, the model behavior we show in this analysis provides a suite of more general insights. As long as there is an inverse relationship between mean runoff and daily runoff variability (e.g., Molnar et al., 2006; Rossi et al., 2016) and erosional thresholds are large relative to characteristic discharge (e.g., Lague et al., 2005; Tucker, 2004), then the dynamics of our model simulations apply. To help isolate the role of integrating snowmelt statistics with rainfall runoff ones, we ran an additional suite of models that removes the chain of reasoning used to account for snowmelt. Specifically, these

additional model runs (referred to as Rain Only) use a single relationship between mean runoff and variability based on the WaterGAP3 analysis but that ignores the role of SF (Figure S6 in Supporting Information S1). For this set of experiments, we still use the regional relationships between local relief and runoff as baselines cases but ignore relationships between maximum elevation and SF. We consider both linked and unlinked scenarios using the Greater Caucasus and British Columbia rulesets. In the earlier runs, the Greater Caucasus models barely entered into the snowmelt-dominated regime whereas, at high uplift rates, the British Columbia models were well into the snowmelt dominated regime (e.g., Figure 4c).

The suite of Rain Only models highlight again that whether a model is linked or unlinked dominates the nature of the k_{sn}-E relationship (Figure 12a). Comparing the original and Rain Only Greater Caucasus models reveals very minor differences in the nonlinearity of the k_{sn}-E relationship. Comparison of the British Columbia original and Rain Only models reveals a more substantial difference in nonlinearity for the unlinked cases. The original models that included snowmelt are more nonlinear (i.e., higher n) than the Rain Only models. However, the Rain Only models are still extremely nonlinear (e.g., $n = 12$). Together, this suite of models strongly suggests that the dominant controls on the nature of the k_{sn}-E relationship are: (a) the development of an orographic gradient in both mean runoff and variability—which may be influenced by, but does not require, a transition to snowmelt hydrology, and (b) the spatial scale of runoff events.

Finally, it is worth highlighting that because the snowmelt transition is elevation dependent and BL is fixed to zero in all runs, our results represent a minimum effect of snowmelt for a given stream length. The snowmelt transition would be more dominant if either stream profiles were longer or if we considered streams that represented catchments in ranges that drain to other base levels. We illustrate the importance of this assumption using a limited suite of unlinked model runs at 1 mm/yr uplift rates for the Greater Caucasus and British Columbia hydroclimatic rulesets, but where we set the local BL to either 1,000 or 2,000 m (Figures 12c–12g). For the Greater Caucasus rules, raising the BL to 1 and 2 km decreases the catchment averaged k_{sn} by 8.8% and 18.6%, respectively, compared to the 0 km baselevel. For the British Columbia hydroclimatic rules, raising the BL by 1 km decreases k_{sn} by 14.1%. Because almost of all the profile is in the snowmelt dominated regime at 1 km (Figure 12e), raising the baselevel to 2 km leads to a similar reduction in k_{sn} of 14.3%. The reduction in k_{sn} from increasing snowmelt contribution at a constant uplift rate is a direct outcome of the increasing value of both the mean runoff and the shape parameter, thus leading to a general increase in the sublinearity of the k_{sn}-erosion rate relationship.

6.3. Implications on Climate-Tectonic Coupling

We undertook this analysis to understand how orographic gradients in mean runoff and daily runoff variability alter predictions for the topographic evolution of mountain ranges as they grow (e.g., Figure 1). Specifically, we focused on the important transition from rainfall-dominated probability distributions to snowmelt-dominated ones as topography grows, based on our own findings in the Greater Caucasus (Forte et al., 2022). Analysis of WaterGAP3 model data revealed that these hydrological transitions may be generally important to mid-latitude mountain ranges where glacial erosion is limited (Forte & Rossi, 2024b). Our new 1D model of river incision shows that if such orographic gradients are honored, then it is relatively easy to generate highly sub-linear ($5 < n < 16$) relationships between channel steepness and erosion rates. We also found that this model behavior is generalizable, only requiring that variability is inversely correlated with mean runoff and that there are orographic gradients in mean runoff. Snowmelt can act as an amplifier of this effect but is not required.

Assuming a constant set of hydroclimatic variables as mountain ranges grow is likely unrealistic, leading us to argue that increasingly sublinear relationships between topography and erosion may be the norm and not the exception. Early hypotheses on climate-tectonic feedbacks assumed that the most important orographic effects are in extracting precipitation on the windward side and diminishing precipitation on the leeward size of topographic barriers (e.g., Beaumont et al., 1992; Whipple & Meade, 2006; Willett, 1999). Subsequent efforts focused on the importance of mountain topography setting the spatial distribution of precipitation (Roe et al., 2003) and phase of precipitation in mountain landscapes (Anders et al., 2008). While all these orographic effects are undoubtedly important, our model simulations provide a natural progression to these insights by also accounting for how stochastic runoff generation (DiBiase & Whipple, 2011; Lague et al., 2005; Tucker, 2004) will itself be a function of the relief evolution of mountain ranges. Our results highlight that a critical, and largely ignored, set of

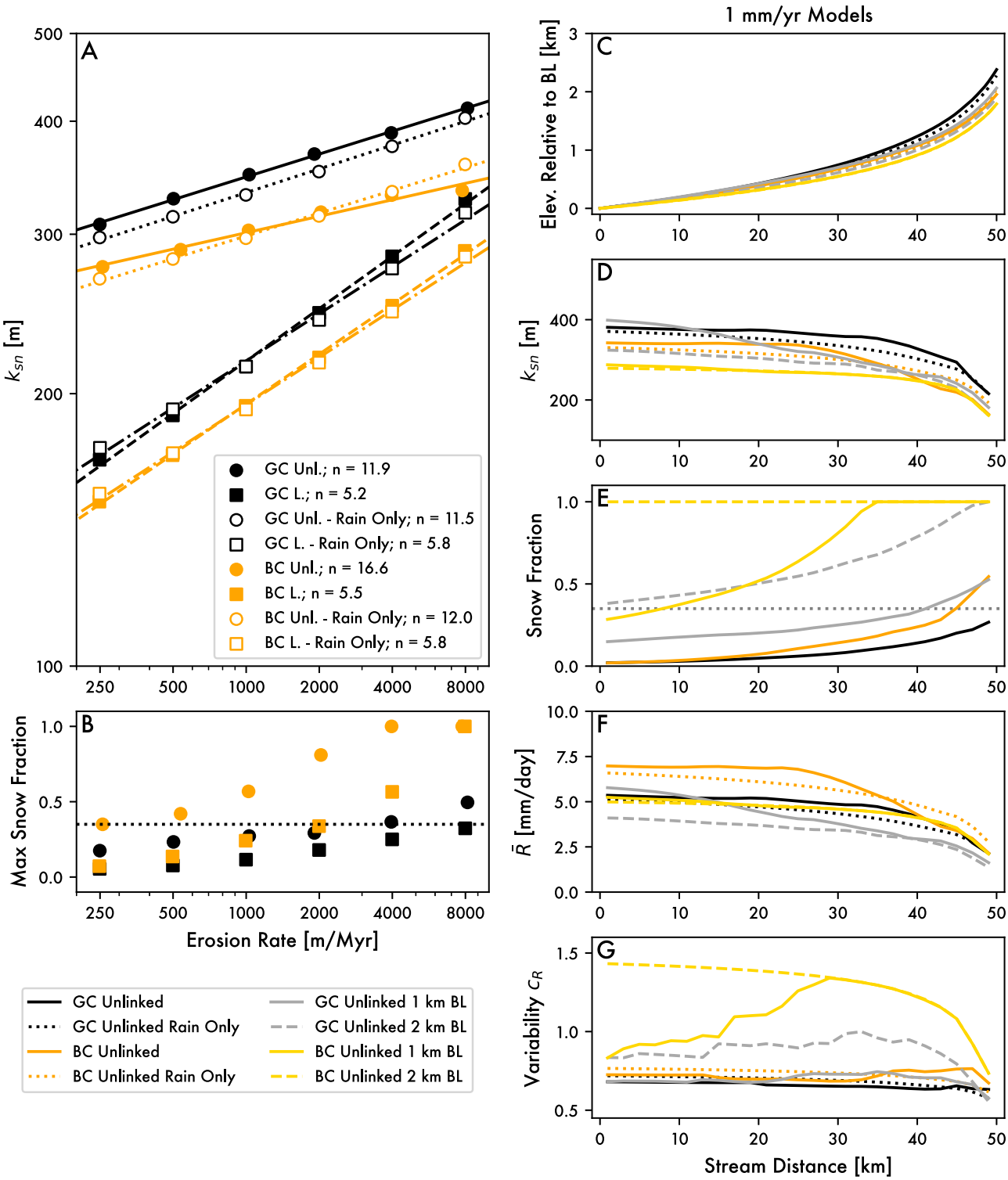

Figure 12. Comparison of Rain Only models and the influence of base level (BL). (a) Erosion rate versus k_{sn} and relevant power law fits for unlinked and linked models for the Greater Caucasus and British Columbia compared against similar runs using the Rain Only model. (b) Maximum snow fraction as a function of erosion rate for scenarios that include snowmelt fraction in ruleset. Right column compares along-profile variation in panel (c) Elevation relative to imposed BL, (d) k_{sn}, (e) Snow fraction, (f) Mean runoff, and (g) Variability. All models on right column were run with a 1 mm/yr uplift rate and are unlinked. This compares the regular models (set to a BL of 0), rain only models (set to a BL of 0), and a suite of models with BL to set to either 1 or 2 km.

parameters associated with the scale of runoff events with respect to watershed size may be fundamental to understanding potential feedbacks between climate and tectonics.

6.4. Limitations and Future Directions

While our new model provides important insights into how orographic gradients in runoff generation can impact stream-power based predictions for topographic relief, there are several important limitations to our model analysis. First, we only use modern relationships between local relief, mean runoff, maximum elevation, and SF at select locations to drive model scenarios. Related to this is the assumption that the observed relationships will persist across geologically long periods of time, even though we know that mean precipitation varies across climate cycles, including glacial-interglacial forcing (e.g., Cruz et al., 2005; Wang et al., 2008). As such, we would expect that both mean runoff, runoff variability, and SF should all vary across glacial-interglacial cycles or larger climate transitions. The impact of these fluctuations will be a function of both the elevation range of the orogen in question, but also its latitude. One novelty of our model is that it makes the rules that describe how hydroclimatology will coevolve with topographic relief explicit. To take advantage of this model feature in simulating glacial-interglacial cycles, we need more detailed accounting for how these cycles impact mean runoff and daily runoff variability through time. Second, in some locations, as elevations and snow accumulation increases, glaciers will begin to develop. In such settings, we would expect a transition from rainfall-dominated fluvial processes to snowmelt-dominated fluvial processes to glacial-dominated processes as mountain ranges grow. We similarly expect that the relative balance of these processes will fluctuate according to interglacial-glacial cycles and/or climate transitions. We do not model the impact of glaciers here, but this would be an important extension, especially in higher latitude locations. As such, our results are most relevant to orogens that do not fully transition into being dominated by glacial erosion during glacial-interglacial cycles. Third, the assumption of static relationships between hydroclimatic and topographic variables assumes that these relationships are valid through all parts of a transient topographic response. In reality, changing topography could impart more complicated relationships. Fully addressing this would require something more akin to a 2D model of orographic precipitation and runoff. Fourth, the discrete boundaries imposed by binning the river profile are quite imperfect. Not only does it imply a scale beyond which runoff parameters can be treated independently, it also fixes the location of these event boundaries in space. The arbitrary locations of these bins are likely an unrealistically hard constraint on the event-scale properties of snowmelt- and rainfall-runoff events. Fifth, we make a simplifying assumption that the erosional threshold (Equation 17) is temporally and spatially fixed in all models. In reality, erosional thresholds might be expected to vary in both time and space, for example, as a function of erosion rate and delivery of large blocks to streams from hillslopes (e.g., Shobe et al., 2018). In theory, one could attempt to build similar empirical relationships between topographic, tectonic, or hydroclimatic parameters in the model to also vary the threshold in a sensible way, making it an important future research direction.

Keeping these limitations in mind, we highlight a few promising directions for future modeling and data analysis on this topic. As computational power increases, we are seeing more realistic simulations of orographic precipitation in bedrock river incision modeling (e.g., Han et al., 2015; Shen et al., 2021). Our results suggest that these efforts would benefit from bringing commensurate improvement in the land surface models that convert precipitation to runoff. For mid-latitude mountain landscapes, it is important to honor the importance of precipitation phase on orographic gradients in runoff patterns (e.g., Anders et al., 2008; Forte et al., 2022; Rossi et al., 2020). Similarly, prior studies highlight the potential importance of Milankovitch forcings on precipitation for landscape evolution (Godard et al., 2013). How these cyclical variations of precipitation are then converted to mean runoff, daily runoff variability, and SF is thus an important unknown. Our focus on the form of k_{sn}-E relationships suggests that a natural extension of this work should also be to examine how spatial-STIM might alter coupled models between climate and tectonics. Relatively simple analytical approaches to this problem (Whipple & Meade, 2004, 2006), as well as more complex dynamical models (e.g., Braun & Yamato, 2010; Roe et al., 2006; Stolar et al., 2007), have yielded important insights into potential feedbacks between climate and tectonics. While we can say that the dynamics in our 1D model will act to dampen such feedbacks, the question of how much is still open and deserves more careful study.

Finally, the assumption of spatial autocorrelation of runoff events proved to be the strongest regulator of erosional efficiency in our new model structure. Within the context of a 1D profile model like ours, having events that are stochastic in space and time is challenging, but not insurmountable. As such, we need more hydrological studies that can help us generalize the spatial statistics of rainfall- and snowmelt-runoff events. Promising work

characterizing potentially significant spatial variability in precipitation patterns in high relief landscapes exist (e.g., Anders et al., 2006, 2007; Barros et al., 2000; Campbell & Steenburgh, 2014; Frei & Schär, 1998; Minder et al., 2008), but generalizing these into how this spatial stochasticity is, or is not, reflected in runoff at a similar scale remains unclear. Similarly, the analysis of WaterGAP3 data by Forte and Rossi (2024b) suggested a fundamental relationship between runoff event size and the contribution from snowmelt. Events with larger spatial footprints appear to be dominated by snowmelt events, further highlighting the interconnectedness of many of the parameters we consider. While fully distributed hydrological models come at a high computational cost for landscape evolution studies, statistical descriptions of these dynamics may be tractable over landscape evolution timescales. Furthermore, the way space is represented in 1D river profiles may not be able to fully mimic the spatial statistics of runoff events, thereby requiring 2D landscape evolution modeling. The Landlab modeling library (Barnhart et al., 2020; Hobley et al., 2017) already has many of the process components suited to implementing spatial-STIM in a 2D framework. Thus, understanding how well we have captured spatiotemporal stochasticity using the assumptions of our 1D model is an important open question that should be tested in 2D (Tucker, 2004; Tucker & Bras, 2000). Despite the clear needs for refining and understanding the applicability of spatial-STIM, our findings show that simply accounting for spatial variations in daily runoff variability is an important step toward generating testable predictions for the erosion laws used by our community.

7. Conclusions

Results from simulations using our new empirically driven 1D profile model that considers both temporal and spatial stochasticity in runoff and snowmelt events highlight that generally sublinear relationships between channel steepness and erosion rate are an expected outcome of orographic development within mountain ranges. Specifically, because of the linkage between mean runoff and runoff variability, the development of orographic gradients in runoff statistics should be expected. Such feedbacks may also be strengthened by the tendency for the increasing elevation of mountain ranges to preferentially accumulate snow, driving a greater component of runoff to be related to snowmelt, and further reducing the variability of runoff. Given the expectation that decreasing runoff variability should lead to increasingly sublinear channel steepness erosion rate relationships, this implies a potential negative feedback on the topographic growth of mountain ranges, providing a process-based explanation for the observation of pseudo-thresholds in channel steepness erosion rate relationships. While basic aspects of this are expected and predictable from prior analyses using STIM, we show here that orographic gradients in mean runoff and variability change fundamental details of model predictions.

A critical outcome of our model results is also that a fundamental parameter for controlling the nature of channel steepness erosion rate relationships is the extent to which the probability of exceedance of runoff events within a given catchment is linked or unlinked. These two endmember states roughly correspond to the extent to which runoff generating events in a given catchment tend to be dominated by spatially restricted convective storm events or larger-scale synoptic events. All other things equal, unlinked scenarios predict steeper landscapes than the equivalent linked scenarios. This implies a fundamental scale dependence on the nature of the relationship between channel steepness and erosion rates. For a given set of hydroclimatological parameters the resulting channel steepness erosion rate pattern can be fit by a simple stream power relationship. However, the extent to which this is meaningful in real data sets, where linked and unlinked dynamics are ignored, is unclear. Ultimately, our results have important implications not only for our understanding of expected coupling between hydroclimatology, topography, and tectonics as a mountain range grows, but also the type of observations we as a community should be considering within our data sets. Future work should focus on considering the implications of spatial and temporal stochasticity of runoff and snowmelt events. There is also a great need for better empirical quantification of the characteristic spatial and temporal scale of runoff events within mountainous catchments and how they evolve with time through glacial-interglacial cycles.

Data Availability Statement

Analysis and model codes necessary to reproduce this work are available in Forte (2024). All model results, additional figures summarizing the results of each model run, and larger outputs of the processing steps are available in Forte and Rossi (2024a). Portions of these analysis codes rely on publicly available data sets that we do not have permission to redistribute, but when used, we provide comments in the code referencing where these data sets can be downloaded.

Acknowledgments
Support for M.W. Rossi came from the Geomorphology and Land-use Dynamics (GLD) Program (EAR-1822062). Neither AMF nor MWR have any real or perceived financial or other conflicts with the contents of this work. We thank Mikael Attal for editorial handling. We also thank Associate Editor Liran Goren and reviewers Eric Deal, Alison Anders, and an anonymous reviewer for probing comments that improved this work.

References

Adams, B. A., Whipple, K. X., Forte, A. M., Heimsath, A. M., & Hodges, K. V. (2020). Climate controls on erosion in tectonically active landscapes. *Science Advances*, *6*(42). https://doi.org/10.1126/sciadv.aaz3166

Ahnert, F. (1970). Functional relationships between denudation, relief, and uplift in large mid-latitude drainage basins. *American Journal of Science*, *268*(3), 243–263. https://doi.org/10.2475/ajs.268.3.243

Alcamo, J., Döll, P., Henrichs, T., Kaspar, F., Lehner, B., Rösch, T., & Siebert, S. (2003). Development and testing of the WaterGAP 2 global model of water use and availability. *Hydrological Sciences Journal*, *48*(3), 317–337. https://doi.org/10.1623/hysj.48.3.317.45290

Anders, A. M., Roe, G. H., Durran, D. R., & Minder, J. R. (2007). Small-scale spatial gradients in climatological precipitation on the Olympic Peninsula. *Journal of Hydrometeorology*, *8*(5), 1068–1081. https://doi.org/10.1175/JHM610.1

Anders, A. M., Roe, G. H., Hallet, B., Montgomery, D. R., Finnegan, N. J., & Putkonen, J. (2006). Spatial patterns of precipitation and topography in the Himalaya. In S. D. Willett, N. Hovius, M. T. Brandon, & D. M. Fisher (Eds.), *Tectonics, climate, and landscape evolution*. Geological Society of America. https://doi.org/10.1130/2006.2398(03)

Anders, A. M., Roe, G. H., Montgomery, D. R., & Hallet, B. (2008). Influence of precipitation phase on the form of mountain ranges. *Geology*, *36*(6), 479. https://doi.org/10.1130/G24821A.1

Barnhart, K. R., Hutton, E. W. H., Tucker, G. E., Gasparini, N. M., Istanbulluoglu, E., Hobley, D. E. J., et al. (2020). Short communication: Landlab v2.0: A software package for Earth surface dynamics. *Earth Surface Dynamics*, *8*(2), 379–397. https://doi.org/10.5194/esurf-8-379-2020

Barros, A. P., Joshi, M., Putkonen, J., & Burbank, D. W. (2000). A study of the 1999 monsoon rainfall in a mountainous region in central Nepal using TRMM products and rain gauge observations. *Geophysical Research Letters*, *27*(22), 3683–3686. https://doi.org/10.1029/2000GL011827

Beaumont, C., Fullsack, P., & Hamilton, J. (1992). Erosional control of active compressional orogens. In K. R. McClay (Ed.), *Thrust tectonics* (pp. 1–18). Chapman Hall.

Binnie, S. A., Phillips, W. M., Summerfield, M. A., & Fifield, L. K. (2007). Tectonic uplift, threshold hillslopes, and denudation rates in a developing mountain range. *Geology*, *35*(8), 743–746. https://doi.org/10.1130/G23641A.1

Bookhagen, B., & Burbank, D. (2006). Topography, relief, and TRMM-derived rainfall variations along the Himalaya. *Geophysical Research Letters*, *33*(8), L08405. https://doi.org/10.1029/2006GL026037

Bookhagen, B., & Burbank, D. (2010). Toward a complete Himalayan hydrological budget: Spatiotemporal distribution of snowmelt and rainfall and their impact on river discharge. *Journal of Geophysical Research*, *115*(F03019). https://doi.org/10.01029/02009JF001426

Bookhagen, B., & Strecker, M. R. (2008). Orographic barriers, high-resolution TRMM rainfall, and relief variations in the eastern Andes. *Geophysical Research Letters*, *35*(L06403). https://doi.org/10.1029/2007GL032011

Botter, G., Porporato, A., Rodriguez-Iturbe, I., & Rinaldo, A. (2009). Nonlinear storage-discharge relations and catchment streamflow regimes: Streamflow regimes of nonlinear catchment. *Water Resources Research*, *45*(10). https://doi.org/10.1029/2008WR007658

Braun, J., & Yamato, P. (2010). Structural evolution of a three-dimensional, finite-width crustal wedge. *Tectonophysics*, *484*(1–4), 181–192. https://doi.org/10.1016/j.tecto.2009.08.032

Campbell, L. S., & Steenburgh, W. J. (2014). Finescale orographic precipitation variability and gap-filling radar potential in little cottonwood Canyon, Utah. *Weather and Forecasting*, *29*(4), 912–935. https://doi.org/10.1175/WAF-D-13-00129.1

Campforts, B., Vanacker, V., Herman, F., Vanmaercke, M., Schwanghart, W., Tenorio, G. E., et al. (2020). Parameterization of river incision models requires accounting for environmental heterogeneity: Insights from the tropical Andes. *Earth Surface Dynamics*, *8*(2), 447–470. https://doi.org/10.5194/esurf-8-447-2020

Cosma, S., Richard, E., & Miniscloux, F. (2002). The role of small-scale orographic features in the spatial distribution of precipitation. *Quarterly Journal of the Royal Meteorological Society*, *128*(579), 75–92. https://doi.org/10.1256/00359000260498798

Coulthard, T. J., & Skinner, C. J. (2016). The sensitivity of landscape evolution models to spatial and temporal rainfall resolution. *Earth Surface Dynamics*, *4*(3), 757–771. https://doi.org/10.5194/esurf-4-757-2016

Crosby, B. T., & Whipple, K. X. (2006). Knickpoint initiation and distribution within fluvial networks: 236 waterfalls in the Waipaoa River, North Island, New Zealand. *Geomorphology*, *82*(1–2), 16–38. https://doi.org/10.1016/j.geomorph.2005.08.023

Cruz, F. W., Burns, S. J., Karmann, I., Sharp, W. D., Vuille, M., Cardoso, A. O., et al. (2005). Insolation-driven changes in atmospheric circulation over the past 116,000 years in subtropical Brazil. *Nature*, *434*(7029), 63–66. https://doi.org/10.1038/nature03365

Cyr, A. J., Granger, D. E., Olivetti, V., & Molin, P. (2010). Quantifying rock uplift rates using channel steepness and cosmogenic nuclide-determined erosion rates: Examples from northern and southern Italy. *Lithosphere*, *2*(3), 188–198. https://doi.org/10.1130/l96.1

Deal, E., Braun, J., & Botter, G. (2018). Understanding the role of rainfall and hydrology in determining fluvial erosion efficiency. *Journal of Geophysical Research: Earth Surface*, *123*(4), 744–778. https://doi.org/10.1002/2017JF004393

Desormeaux, C., Godard, V., Lague, D., Duclaux, G., Fleury, J., Benedetti, L., & Bellier, O. (2022). Investigation of stochastic-threshold incision models across a climatic and morphological gradient. *Earth Surface Dynamics*, *10*(3), 473–492. https://doi.org/10.5194/esurf-10-473-2022

DiBiase, R. A., & Whipple, K. X. (2011). The influence of erosion thresholds and runoff variability on the relationships among topography, climate, and erosion rate. *Journal of Geophysical Research*, *116*(F04036), F04036. https://doi.org/10.1029/2011JF002095

DiBiase, R. A., Whipple, K. X., Heimsath, A. M., & Ouimet, W. B. (2010). Landscape form and millennial erosion rates in the San Gabriel Mountains, CA. *Earth and Planetary Science Letters*, *289*(1–2), 134–144. https://doi.org/10.1016/j.epsl.2009.10.036

Döll, P., Kaspar, F., & Lehner, B. (2003). A global hydrological model for deriving water availability indicators: Model tuning and validation. *Journal of Hydrology*, *270*(1–2), 105–134. https://doi.org/10.1016/S0022-1694(02)00283-4

Dunne, T., & Black, R. D. (1970). Partial area contributions to storm runoff in a small New England watershed. *Water Resources Research*, *6*(5), 1296–1311. https://doi.org/10.1029/WR006i005p01296

Farr, T. G., Rosen, P. A., Caro, E., Crippen, R., Duren, R., Hensley, S., et al. (2007). The shuttle radar topography mission. *Reviews of Geophysics*, *45*(2), 1–33. https://doi.org/10.1029/2005rg000183

Ferrier, K. L., Huppert, K. L., & Perron, J. T. (2013). Climatic control of bedrock river incision. *Nature*, *496*(7444), 206–209. https://doi.org/10.1038/nature11982

Flint, J. J. (1974). Stream gradient as a function of order, magnitude, and discharge. *Water Resources Research*, *10*(5), 969–973. https://doi.org/10.1029/wr010i005p00969

Forte, A. M. (2024). amforte/snowmelt_orography: Snowmelt Orography (Version v2.0). *Zenodo*. https://doi.org/10.5281/zenodo.10449397

Forte, A. M., Leonard, J. S., Rossi, M. W., Whipple, K. X., Heimsath, A. M., Sukhishvili, L., et al. (2022). Low variability runoff inhibits coupling of climate, tectonics, and topography in the Greater Caucasus. *Earth and Planetary Science Letters*, *584*, 117525. https://doi.org/10.1016/j.epsl.2022.117525

Forte, A. M., & Rossi, M. W. (2024a). Data and model results associated with stochastic in space and time: Parts 1 and 2 (Version 2.0) [Dataset]. https://doi.org/10.5281/zenodo.10407347

Forte, A. M., & Rossi, M. W. (2024b). Stochastic in space and time: Part 1, characterizing orographic gradients in mean runoff and daily runoff variability. *Journal of Geophysical Research F: Earth Surface*. https://doi.org/10.1029/2023JF007326

Forte, A. M., & Whipple, K. X. (2019). Short communication: The Topographic Analysis Kit (TAK) for TopoToolbox. *Earth Surface Dynamics*, *7*(1), 87–95. https://doi.org/10.5194/esurf-7-87-2019

Forte, A. M., Whipple, K. X., Bookhagen, B., & Rossi, M. W. (2016). Decoupling of modern shortening rates, climate, and topography in the Caucasus. *Earth and Planetary Science Letters*, *449*, 282–294. https://doi.org/10.1016/j.epsl.2016.06.013

Frei, C., & Schär, C. (1998). A precipitation climatology of the Alps from high-resolution rain-gauge observations. *International Journal of Climatology*, *18*(8), 873–900. https://doi.org/10.1002/(SICI)1097-0088(19980630)18:8<873::AID-JOC255>3.0.CO;2-9

Gallen, S. F., & Fernández-Blanco, D. (2021). A new data-driven Bayesian inversion of fluvial topography clarifies the tectonic history of the corinth rift and reveals a channel steepness threshold. *Journal of Geophysical Research: Earth Surface*, *126*(3). https://doi.org/10.1029/2020JF005651

Garvert, M. F., Smull, B., & Mass, C. (2007). Multiscale mountain waves influencing a major orographic precipitation event. *Journal of the Atmospheric Sciences*, *64*(3), 711–737. https://doi.org/10.1175/JAS3876.1

Gasparini, N. M., & Brandon, M. T. (2011). A generalized power law approximation for fluvial incision of bedrock channels. *Journal of Geophysical Research*, *116*(F2). https://doi.org/10.1029/2009JF001655

Godard, V., Tucker, G. E., Fisher, G. B., Burbank, D. W., & Bookhagen, B. (2013). Frequency-dependent landscape response to climatic forcing. *Geophysical Research Letters*, *40*(5), 859–863. https://doi.org/10.1002/grl.50253

Hack, J. T. (1957). Studies of longitudinal stream profiles in Virginia and Maryland (pp. 97).

Han, J., Gasparini, N. M., & Johnson, J. P. L. (2015). Measuring the imprint of orographic rainfall gradients on the morphology of steady-state numerical fluvial landscapes: Orographic rainfall and steady-state fluvial landscapes. *Earth Surface Processes and Landforms*, *40*(10), 1334–1350. https://doi.org/10.1002/esp.3723

Harel, M. A., Mudd, S. M., & Attal, M. (2016). Global analysis of the stream power law parameters based on worldwide 10Be denudation rates. *Geomorphology*, *268*, 184–196. https://doi.org/10.1016/j.geomorph.2016.05.035

Harkins, N., Kirby, E., Heimsath, A. M., Robinson, R., & Reiser, U. (2007). Transient fluvial incision in the headwaters of the Yellow River, northeastern Tibet, China. *Journal of Geophysical Research*, *112*(F3), F03S04. https://doi.org/10.1029/2006jf000570

Hilley, G. E., Porder, S., Aron, F., Baden, C. W., Johnstone, S. A., Liu, F., et al. (2019). Earth's topographic relief potentially limited by an upper bound on channel steepness. *Nature Geoscience*, *12*(10), 828–832. https://doi.org/10.1038/s41561-019-0442-3

Hobley, D. E. J., Adams, J. M., Nudurupati, S. S., Hutton, E. W. H., Gasparini, N. M., Istanbulluoglu, E., & Tucker, G. E. (2017). Creative computing with Landlab: An open-source toolkit for building, coupling, and exploring two-dimensional numerical models of Earth-surface dynamics. *Earth Surface Dynamics*, *5*(1), 21–46. https://doi.org/10.5194/esurf-5-21-2017

Howard, A. D. (1994). A detachment-limited model of drainage basin evolution. *Water Resources Research*, *30*(7), 2261–2285. https://doi.org/10.1029/94wr00757

Kirby, E., & Whipple, K. X. (2012). Expression of active tectonics in erosional landscapes. *Journal of Structural Geology*, *44*, 54–75. https://doi.org/10.1016/j.jsg.2012.07.009

Lague, D. (2014). The stream power river incision model: Evidence, theory and beyond. *Earth Surface Processes and Landforms*, *39*(1), 38–61. https://doi.org/10.1002/esp.3462

Lague, D., Hovius, N., & Davy, P. (2005). Discharge, discharge variability, and the bedrock channel profile. *Journal of Geophysical Research*, *110*(F4), F04006. https://doi.org/10.1029/2004JF000259

Lehner, B., Verdin, K., & Jarvis, A. (2008). New global hydrography derived from spaceborne elevation data. *Eos, Transactions American Geophysical Union*, *89*(10), 93–94. https://doi.org/10.1029/2008EO100001

Leonard, J. S., Whipple, K. X., & Heimsath, A. M. (2023a). Controls on topography and erosion of the north-central Andes. *Geology*, *52*(2), 153–158. https://doi.org/10.1130/G51618.1

Leonard, J. S., Whipple, K. X., & Heimsath, A. M. (2023b). Isolating climatic, tectonic, and lithologic controls on mountain landscape evolution. *Science Advances*, *9*(3), eadd8915. https://doi.org/10.1126/sciadv.add8915

Marder, E., & Gallen, S. F. (2023). Climate control on the relationship between erosion rate and fluvial topography. *Geology*, *51*(5), 424–427. https://doi.org/10.1130/G50832.1

Marra, F., Armon, M., & Morin, E. (2022). Coastal and orographic effects on extreme precipitation revealed by weather radar observations. *Hydrology and Earth System Sciences*, *26*(5), 1439–1458. https://doi.org/10.5194/hess-26-1439-2022

Miller, S. R., Sak, P. B., Kirby, E., & Bierman, P. R. (2013). Neogene rejuvenation of central Appalachian topography: Evidence for differential rock uplift from stream profiles and erosion rates. *Earth and Planetary Science Letters*, *369*, 1–12. https://doi.org/10.1016/j.epsl.2013.04.007

Minder, J. R., Durran, D. R., Roe, G. H., & Anders, A. M. (2008). The climatology of small-scale orographic precipitation over the Olympic Mountains: Patterns and processes. *Quarterly Journal of the Royal Meteorological Society*, *134*(633), 817–839. https://doi.org/10.1002/qj.258

Molnar, P., Anderson, R. S., Kier, G., & Rose, J. (2006). Relationships among probability distributions of stream discharges in floods, climate, bed load transport, and river incision. *Journal of Geophysical Research*, *111*(F2), F02001. https://doi.org/10.1029/2005JF000310

Montgomery, D. R., & Brandon, M. T. (2002). Topographic controls on erosion rates in tectonically active mountain ranges. *Earth and Planetary Science Letters*, *201*(3–4), 481–489. https://doi.org/10.1016/s0012-821x(02)00725-2

Olivetti, V., Cyr, A. J., Molin, P., Faccenna, C., & Granger, D. E. (2012). Uplift history of the Sila Massif, southern Italy, deciphered from cosmogenic Be-10 erosion rates and river longitudinal profile analysis. *Tectonics*, *31*(3), TC3007. https://doi.org/10.1029/2011TC003037

Ouimet, W. B., Whipple, K. X., & Granger, D. E. (2009). Beyond threshold hillslopes: Channel adjustment to base-level fall in tectonically active mountain ranges. *Geology*, *37*(7), 579–582. https://doi.org/10.1130/g30013a.1

Peleg, N., Skinner, C., Ramirez, J. A., & Molnar, P. (2021). Rainfall spatial-heterogeneity accelerates landscape evolution processes. *Geomorphology*, *390*, 107863. https://doi.org/10.1016/j.geomorph.2021.107863

Perron, J. T., & Royden, L. H. (2013). An integral approach to bedrock river profile analysis. *Earth Surface Processes and Landforms*, *38*(6), 570–576. https://doi.org/10.1002/esp.3302

Roe, G. H. (2005). Orographic precipitation. *Annual Review of Earth and Planetary Sciences*, *33*(1), 645–671. https://doi.org/10.1146/annurev.earth.33.092203.122541

Roe, G. H., Montgomery, D. R., & Hallet, B. (2002). Effects of orographic precipitation variations on the concavity of steady-state river profiles. *Geology*, *30*(2), 143–146. https://doi.org/10.1130/0091-7613(2002)030<0143:eoopvo>2.0.co;2

Roe, G. H., Montgomery, D. R., & Hallet, B. (2003). Orographic precipitation and the relief of mountain ranges. *Journal of Geophysical Research*, *108*(B6). https://doi.org/10.1029/2001JB001521

Roe, G. H., Stolar, D. B., & Willett, S. D. (2006). Response of a steady-state critical wedge orogen to changes in climate and tectonic forcing. In S. D. Willett, N. Hovius, M. T. Brandon, & D. Fisher (Eds.), *Tectonics, climate, and landscape evolution* (Vols. 1–398, pp. 239–272).

Rosenbloom, N., & Anderson, R. S. (1994). Hillslope and channel evolution in a marine terraced landscape, Santa Cruz, California. *Journal of Geophysical Research*, *99*(B7), 14013–14029. https://doi.org/10.1029/94jb00048

Rossi, M. W., Anderson, R. S., Anderson, S. P., & Tucker, G. E. (2020). Orographic controls on subdaily rainfall statistics and flood frequency in the Colorado Front Range, USA. *Geophysical Research Letters*, *47*(4). https://doi.org/10.1029/2019GL085086

Rossi, M. W., Quigley, M. C., Fletcher, J. M., Whipple, K. X., Díaz-torres, J. J., Seiler, C., et al. (2017). Along-strike variation in catchment morphology and cosmogenic denudation rates reveal the pattern and history of footwall uplift, Main Gulf Escarpment, Baja California. *Geological Society of America Bulletin*, *129*(7–8), 837–854. https://doi.org/10.1130/B31373.1

Rossi, M. W., Whipple, K. X., & Vivoni, E. R. (2016). Precipitation and evapotranspiration controls on event-scale runoff variability in the contiguous United States and Puerto Rico. *Journal of Geophysical Research*, *121*(1), 128–145. https://doi.org/10.1002/2015JF003446

Safran, E. B., Bierman, P. R., Aalto, R., Dunne, T., Whipple, K. X., & Caffee, M. W. (2005). Erosion rates driven by channel network incision in the Bolivian Andes. *Earth Surface Processes and Landforms*, *30*(8), 1007–1024. https://doi.org/10.1002/esp.1259

Sassolas-Serrayet, T., Cattin, R., & Ferry, M. (2018). The shape of watersheds. *Nature Communications*, *9*(1), 1–8. https://doi.org/10.1038/s41467-018-06210-4

Schaefli, B., Rinaldo, A., & Botter, G. (2013). Analytic probability distributions for snow-dominated streamflow: Snow-Dominated Streamflow Pdfs. *Water Resources Research*, *49*(5), 2701–2713. https://doi.org/10.1002/wrcr.20234

Scherler, D., Bookhagen, B., & Strecker, M. R. (2014). Tectonic control on 10 Be-derived erosion rates in the Garhwal. *Journal of Geophysical Research: Earth Surface*, *119*(August 2013), 83–105. https://doi.org/10.1002/2013JF002955

Scherler, D., DiBiase, R. A., Fisher, G. B., & Avouac, J.-P. (2017). Testing monsoonal controls on bedrock river incision in the Himalaya and Eastern Tibet with a stochastic-threshold stream power model. *Journal of Geophysical Research: Earth Surface*, *122*(7), 1389–1429. https://doi.org/10.1002/2016JF004011

Schmidt, K. M., & Montgomery, D. R. (1995). Limits to relief. *Science*, *270*(5236), 617–620. https://doi.org/10.1126/science.270.5236.617

Schwanghart, W., & Scherler, D. (2014). Short communication: TopoToolbox 2 – MATLAB based software for topographic analysis and modeling in Earth surface sciences. *Earth Surface Dynamics*, *2*, 1–7. https://doi.org/10.5194/esurf-2-1-2014

Shen, H., Lynch, B., Poulsen, C. J., & Yanites, B. J. (2021). A modeling framework (WRF-Landlab) for simulating orogen-scale climate-erosion coupling. *Computers & Geosciences*, *146*, 104625. https://doi.org/10.1016/j.cageo.2020.104625

Shobe, C. M., Tucker, G. E., & Rossi, M. W. (2018). Variable-threshold behavior in rivers arising from hillslope-derived blocks. *Journal of Geophysical Research: Earth Surface*, *123*(8), 1931–1957. https://doi.org/10.1029/2017JF004575

Snyder, N. P., Whipple, K. X., Tucker, G. E., & Merrits, D. J. (2003). Importance of a stochastic distribution of floods and erosion thresholds in the bedrock river incision problem. *Journal of Geophysical Research*, *108*(B2). https://doi.org/10.1029/2001JB001655

Stolar, D. B., Roe, G. H., & Willett, S. D. (2007). Controls on the patterns of topography and erosion rate in a critical orogen. *Journal of Geophysical Research*, *112*(F04002). https://doi.org/10.1029/2006JF000713

Tucker, G. E. (2004). Drainage basin sensitivity to tectonic and climatic forcing: Implications of a stochastic model for the role of entrainment and erosion thresholds. *Earth Surface Processes and Landforms*, *29*(2), 185–204. https://doi.org/10.1002/esp.1020

Tucker, G. E., & Bras, R. L. (2000). A stochastic approach to modeling the role of rainfall variability in drainage basin evolution. *Water Resources Research*, *36*(7), 1953–1964. https://doi.org/10.1029/2000wr900065

Wang, Y., Cheng, H., Edwards, R. L., Kong, X., Shao, X., Chen, S., et al. (2008). Millennial- and orbital-scale changes in the East Asian monsoon over the past 224,000 years. *Nature*, *451*(7182), 1090–1093. https://doi.org/10.1038/nature06692

Whipple, K. X. (2001). Fluvial landscape response time: How plausible is steady-state denudation? *American Journal of Science*, *301*(4–5), 313–325. https://doi.org/10.2475/ajs.301.4-5.313

Whipple, K. X. (2009). The influence of climate on the tectonic evolution of mountain belts. *Nature Geoscience*, *2*, 97–104. https://doi.org/10.1038/ngeo413

Whipple, K. X., DiBiase, R. A., Crosby, B., & Johnson, J. P. L. (2022). Bedrock rivers. In J. Jack & F. Shroder (Eds.), *Treatise on Geomorphology* (2nd ed., pp. 865–903). Academic Press. https://doi.org/10.1016/B978-0-12-818234-5.00101-2

Whipple, K. X., & Meade, B. (2004). Controls on the strength of coupling among climate, erosion, and deformation in two-sided, frictional orogenic wedges at steady state. *Journal of Geophysical Research*, *109*(F1), F01011. https://doi.org/10.1029/2003JF000019

Whipple, K. X., & Meade, B. (2006). Orogen response to changes in climatic and tectonic forcing. *Earth and Planetary Science Letters*, *243*(1–2), 218–228. https://doi.org/10.1016/j.epsl.2005.12.022

Whipple, K. X., & Tucker, G. E. (1999). Dynamics of the stream-power river incision model: Implications for height limits of mountain ranges, landscape response timescales, and research needs. *Journal of Geophysical Research*, *104*(B8), 17661–17674. https://doi.org/10.1029/1999jb900120

Whipple, K. X., & Tucker, G. E. (2002). Implications of sediment-flux-dependent river incision models for landscape evolution. *Journal of Geophysical Research*, *107*(B2). https://doi.org/10.1029/2000JB000044

Willett, S. D. (1999). Orogeny and orography: The effects of erosion on the structure of mountain belts. *Journal of Geophysical Research*, *104*(B12), 28957–28981. https://doi.org/10.1029/1999jb900248

Wobus, C. W., Whipple, K. X., Kirby, E., Snyder, N. P., Johnson, J., Spyropolou, K., et al. (2006). Tectonics from topography: Procedures, promise, and pitfalls. In S. D. Willett, N. Hovius, M. T. Brandon, & D. Fisher (Eds.), *Tectonics, climate, and landscape evolution* (Vols. 1–398, pp. 55–74). The Geological Society of America.

Wolman, M. G., & Miller, J. P. (1960). Magnitude and frequency of forces in geomorphic processes. *The Journal of Geology*, *68*(1), 54–74. https://doi.org/10.1086/626637

Yanites, B. J., Becker, J. K., Madritsch, H., Schnellmann, M., & Ehlers, T. A. (2017). Lithologic effects on landscape response to base level changes: A modeling study in the context of the eastern Jura Mountains, Switzerland. *Journal of Geophysical Research: Earth Surface*, *122*(11), 2196–2222. https://doi.org/10.1002/2016JF004101